NOTE TO USERS

Non-Destructive Characterization of Stony Meteorites

By

Darren L. Smith

A thesis submitted to the
Faculty of Graduate Studies and Research
in partial fulfillment of the requirements for the degree of
Master of Science, Department of Earth Sciences

Carleton University
Ottawa, Ontario
December 2005

Your file Votre référence
ISBN: 0-494-13471-2
Our file Notre référence
ISBN: 0-494-13471-2

Abstract

The characterization of meteoritic material is of fundamental importance to our understanding of the solar system and its processes of formation. Many meteorites are small, fragile and unique and thus the identification and subsequent preservation of this material is a priority. The present study investigates two non-destructive techniques of meteorite characterization and classification.

A new method of density determination and surface roughness description using 3D laser imaging has been evaluated on eleven stony meteorites. In addition, four magnetic parameters that show promise as classification tools were evaluated on 321 stony meteorite specimens: bulk magnetic susceptibility and its frequency dependence (825 and 19000 Hz), and the degree and shape of the anisotropy of magnetic susceptibility.

Densities determined using 3D laser imaging compare very well with previously published values. 3D laser imaging is the least invasive method of density measurement currently available and may provide a more accurate estimate of the meteorite's bulk volume than other methods. A measure of surface roughness is proposed using a pilot approach.

Chondrites show a clear trend of increasing bulk susceptibility from LL, L, H to E probably governed by Fe-Ni metal and sulphide content; achondrite values are more varied. Frequency dependence is observed with variations in magnitude among meteorite classes. Degrees of anisotropy range from 1 – 53%. Strong oblate and prolate fabrics are observed among and within meteorite classes of chondritic and achondritic material pointing to a complex, multi-mechanism origin for anisotropy, more so than previously thought, and likely dominated by impact processes in the later stages of stony parent body formation.

Acknowledgements

I foremost like to thank my co-supervisors Claire Samson and Richard Ernst of Carleton University for their guidance during this project. Their openness and availability made this research project a very valuable and enjoyable experience. I also sincerely thank Richard Herd of the Geological Survey of Canada for his additional supervision over the last two years and for allowing access to the National Meteorite Collection of Canada. His great enthusiasm, ideas and guidance were sources of great inspiration.

This research project was generously supported by Neptec Design Group (Ottawa, Canada) through financial contributions and access to instruments and software. Chapter I of this project could not have been achieved without their significant support. Moreover, much appreciation is extended to Adam Deslauriers and Jean-Eric Sink of Neptec for their technical assistance with the Laser Camera System and theory. Thanks are also extended to Iain Christie, Director of Research and Development at Neptec, for overseeing the laser camera phase of the research project and for allowing frequent access to the facilities.

I also like to thank InnovMetric for access to a trial version of Polyworks for data analysis in Chapter I (Part II) and Louis-Jérôme Doyon in particular for his assistance with Chapter I (Part II) on methodology and approach.

Thanks are extended to Pierre Rochette and Luigi Folco for their helpful reviews that strengthened Chapter II (prior to publication in Meteoritics and Planetary Science) and Ann Hirt of the Institute of Geophysics, Zurich for information related to frequency dependence in Chapter II. Much appreciation is also expressed to Ken Buchan of the Geological Survey of Canada for his laboratory assistance during magnetic measurements.

Finally, I like to express my utmost gratitude to my friends and family who have supported me during this research project with their unwavering kindness and interest over the past two years.

Table of Contents

List of Figures

Chapter I (Part I)

Chapter I (Part II)

Chapter II

List of Tables

Chapter I (Part I)

Chapter I (Part II)

Chapter II

List of Appendices

General Introduction

The first documented occurrences of meteorites falling from the sky date back to nearly 2000 BC. These phenomena, however, were long thought to be of atmospheric nature. It was not before several millennia later, in the18th century, that scientists concluded that meteorites were not of terrestrial origin. Since this realization, the characterization of meteorites has been recognized as fundamental to the study of space and planetary sciences. Most meteorites have remained relatively unaltered since their coeval creation with the solar system and therefore their properties reflect their formation conditions within the solar nebula. Meteorites are direct samples of materials from various regions of the solar system allowing for much to be learned about the evolutionary chemical and physical processes leading to its current makeup and zonal structure. Furthermore, as most meteorites are derived from asteroids, they can tell us much about the interiors of these small bodies (e.g. density, porosity, composition, etc.). Meteorites have appreciably high Fe-Ni metal content and thus economic value in addition to their scientific value. Their study provides valuable insight for future exploration and mining endeavors as the Earth's resources are not infinite (Lewis 1996).

The meteorite concentration mechanisms existing in the Antarctic (Cassidy 2003) along with the large number of meteorites being found in desert regions in Asia and Africa have resulted in a huge backlog of unclassified meteorite samples, amounting to several hundred each year. Meteoritic material is a rare scientific resource and the identification of unique samples and their preservation for future study is of paramount importance. There therefore exists a need for a fast, non-destructive and systematic way to characterize the expanding inventory of meteorites being discovered on Earth.

The primary objective of the present study is to demonstrate the use of two non-contaminating and non-destructive techniques of meteorite characterization and classification which preserve the material for further study.

This thesis is divided into two chapters along with a general introduction and a final concluding section.

Chapter I presents an innovative technique of non-destructive volume measurement of meteorites for density determination based on three-dimensional (3D) laser imaging. Volume measurement has previously been difficult to accomplish without alteration or destruction occurring to the sample. An auto-synchronized laser scanner imaged the surface features of eleven meteorite fragments from seven different stony meteorites (five chondrites and two achondrites) of varying shape, size, surface roughness, porosity and reflectance. Visualization software was then used to align several scans into a closed model and to compute its volume. In addition, the image data for the eleven meteorites were also used to develop a semi-quantitative approach of meteorite surface roughness description.

Chapter II focuses on non-destructive meteorite characterization by measurement of magnetic properties. Four parameters of low-field magnetic susceptibility (bulk value, frequency dependence, degree of anisotropy and ellipsoid shape) were evaluated on 321 meteorite specimens and analyzed as classification tools. In addition, fundamental questions about meteorite provenance and parent body history are addressed through the new data obtained.

The present study concentrates on stony meteorites as they represent the vast majority of meteorites being collected and those already present in the collections throughout the world.

Chapter I (Part I)

Measuring the Bulk Density of Meteorites Non-Destructively Using 3D Laser Imaging*

1.0 Introduction

Bulk density, defined as the ratio of material mass over the total volume of mineral grains plus pore space (Bates and Jackson 1987), is a physical parameter that varies among rock types and can provide insight into the origin of rock material. The mass is usually easy to measure with no alteration occurring to the material. Determining the volume of soluble, fragile and/or porous material, however, is a far more difficult task to complete without contamination or harmful alteration occurring to the sample itself. This is especially true for meteorites. Their uniqueness and scarcity require a method of volume measurement that is non-destructive yet accurate.

Conventional methods of volume measurement suffer from various forms of inaccuracy and imprecision, and can severely alter the nature of the material during measurement. Britt and Consolmagno (2003) provide an overview of the various techniques for determining the bulk density of meteorites and also provide a summary of all calculated meteorite densities found in the literature prior to December 2001. Soaking the sample in a fluid and employing Archimedes' Principle, whereby an object submersed in a liquid will displace a volume of liquid equal to the volume of the object itself, is the most widely used technique for meteorites (e.g. Keil 1962; Kukkonen and Pesonen 1983; Terho et al. 1993). Errors, however, can be introduced by fluid entering the pore spaces and irreversible contamination and damage to the sample can occur.

*Chapter I (Part I) is adapted from Smith et al. (2005d)

Another, more recent method uses the displacement of micrometre-size glass beads to imitate the fluid in Archimedes' Principle (e.g. Consolmagno and Britt 1998; Wilkison et al. 2003). Although the technique is non-destructive, it is susceptible to shaking and settling causing a redistribution and compaction of beads, environmental conditions such as temperature and humidity, and errors introduced by different ratios of meteorite volume to container volume (Wilkison and Robinson 2000). Another method goes to such extreme as to cut meteorites into basic shapes (e.g. cubes or thin slabs) to simplify volume measurement. Finally, a variant of this approach consists of packing the meteorite in clay forming an easily measurable shape. The clay is then removed, remolded and remeasured. The difference in measured volumes is the presumed volume of the meteorite.

The above review shows that there is a need for an alternative technique – non-destructive, accurate and precise – for density measurements of meteoritic and other rare material. This chapter presents results of a new non-destructive technique for determining the bulk density of meteorites and other rock samples using 3D image data acquired with the Laser Camera System (LCS), an auto-synchronized laser scanner developed by Neptec Design Group of Ottawa, Canada (http://www.neptec.com). This technique, originally proposed by Herd et al. (2003), has been refined in the present study. Along with aiding in the development of the method, the measured densities will also assist in meteorite characterization as meteorite density can be related to the interior of asteroids and therefore provide information on parent bodies. Eleven fragments from seven different stony meteorites (five chondrites and two achondrites) which vary in shape, size, surface roughness, porosity and reflectance have been imaged and had their densities determined. All of the meteorites studied belong to the National Meteorite Collection of Canada of the Geological Survey of Canada (GSC), Natural Resources Canada.

1.1 Methodology

1.1.1 *Instrumentation*

The LCS is a 3D laser scanner based on an auto-synchronized principle originating from the National Research Council of Canada (Rioux 1984) and further developed for space and terrestrial applications by Neptec Design Group (Samson et al. 2004).

The projected light is a 1500 nm infrared laser beam focused to a spot size of 0.8 mm at a distance of 1.2 m in front of the camera. Two mirrors controlled by high-precision galvanometers deflect the laser beam which scans over the target object in a raster pattern. The diffusely-reflected laser light is then collected through a lens and illuminates a charge-coupled device (CCD) (Fig. 1.1). This photodetector is only sensitive over a narrow range of frequencies (1500±3 nm) centered on the projected light frequency. No special lighting of the target is therefore required and contamination from other light sources is minimal. By triangulating the projected and reflected raypaths, three spatial coordinates (X, Y, Z) are obtained for each voxel imaged, together with the reflection intensity (I). The term "voxel" is used here to describe a volumetric image element, as opposed to the term "pixel" which is a two-dimensional image element. A more detailed description of the auto-synchronized principle can be found in Beraldin et al. (1993). Its practical implementation in the LCS is presented in Samson et al. (2001) and Smith, I. C. et al. (2003). Basic LCS specifications are listed in Table 1.1. At its focusing distance, the LCS has a precision of 100 μm (one standard deviation).

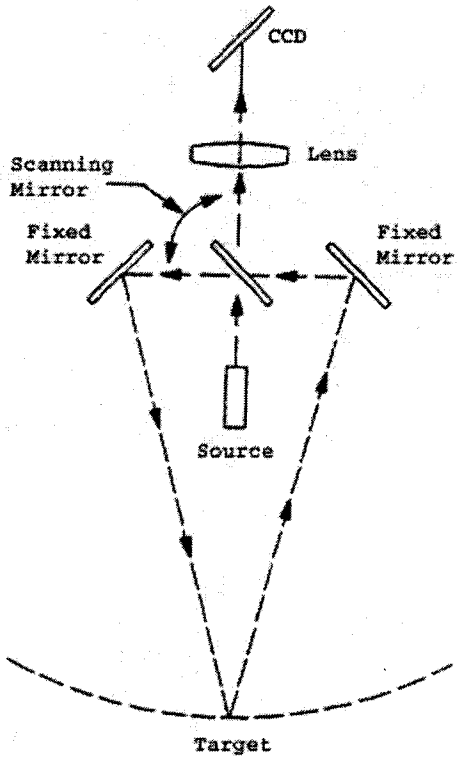

Fig. 1.1. Schematic of the auto-synchronized principle implemented in the Laser Camera System (LCS) (from Beraldin et al. 1993).

Physical characteristics		
Enclosure dimensions	cm^3	18.8 x 25.4 x 27.9
Mass	kg	12.1
General imaging characteristics		
Source wavelength	nm	1500
Detector sensitivity	nm	1500±3
Maximum field of view	degree	30 x 30
Maximum image resolution	voxel	1024 x 1024
Integration time	µs	20 - 500
Maximum acquisition rate	voxel/s	5000
Imaging performance at focusing distance		
Focusing distance	m	1.2
Laser spot size	mm	0.8
Depth resolution	mm	0.5
Precision (1 standard deviation)	µm	100

Table 1.1. LCS specifications.

1.1.2 *Acquisition of 3D Image Data*

Minimal handling of the meteorite was required during the imaging process. The LCS was mounted on a tripod, 1.2 m in front of a pedestal where a meteorite was presented (Fig. 1.2). A scan at a resolution of 512 x 512 voxels was performed in a systematic raster pattern until the surface features within the field of view (30 x 30 degrees) had been imaged. Each imaged element is approximately 1.2 x 1.2 mm in dimension. The elements are spaced widely enough with respect to the spot size (0.8 mm) so that no smearing due to oversampling occurs. An integration time of 180 μs was chosen as it gave the highest overall signal to noise ratio for the eleven meteorites scanned while avoiding detector saturation and minimizing data acquisition time. The meteorite was then rotated, without contact, approximately 60 degrees by means of a turntable and a new scan was performed. This process was repeated six times. After that, the meteorite was physically reoriented in order to image the top and bottom surfaces. Finally, a few additional scans were made to capture sharp edges and minimize shadow effects. Shadow effects occur when the walls of crevasses or cavities obstruct the projected or reflected ray paths of the laser beam (Rioux 1984). A total of nine to twelve scans were required to cover the entire surface area of each meteorite, depending on the size of the meteorite, the extent of any sharp edges present, and shadow effects. Data acquisition took approximately 20-30 minutes to complete per sample. The directly measured voxels, prior to any interpolation or surface construction, are referred to as "point cloud data". In this study, only the X, Y, Z point cloud data were used to build volumetric models, after manual removal of outliers and reflections from the background and turntable. The reflection data (variable I) could be used in the future for studying surface properties such as reflectance and texture. The characteristics of the 3D laser images acquired in this study are listed in Table 1.2.

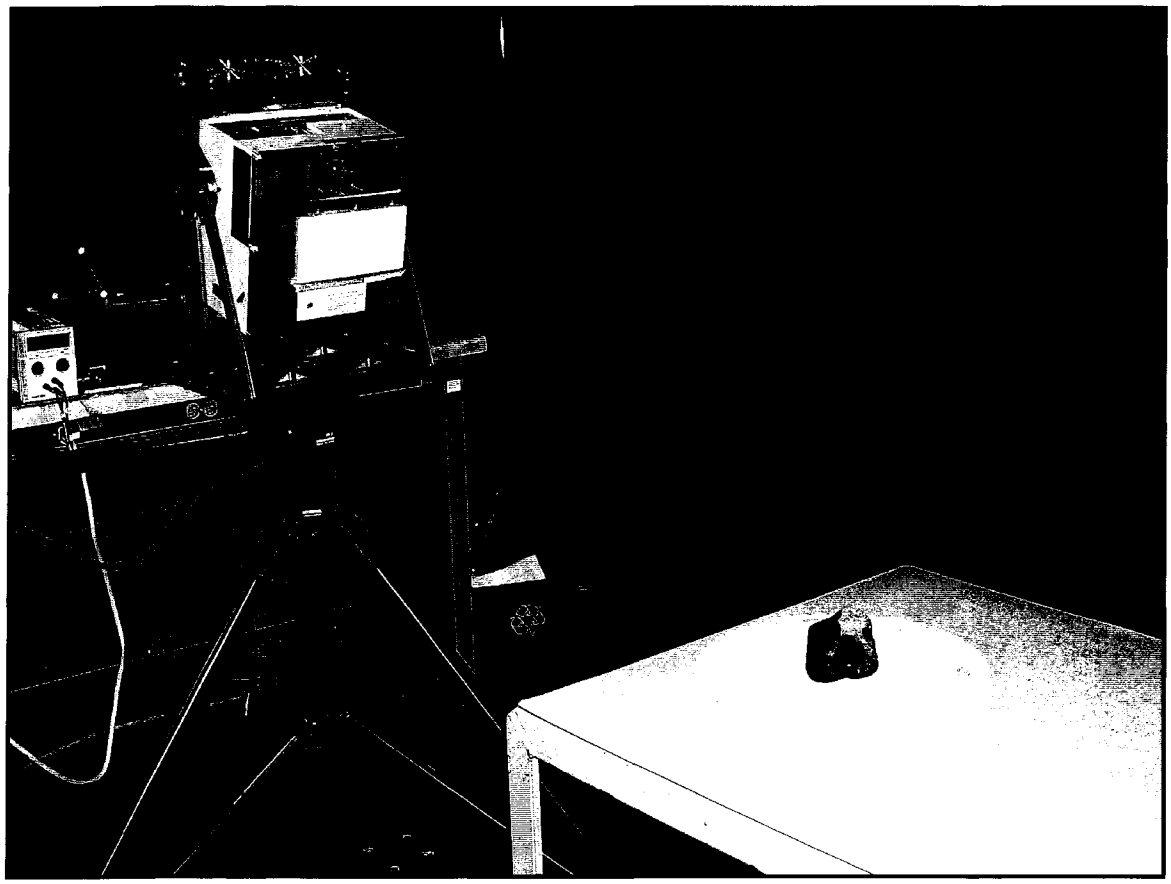

Fig. 1.2. Instrument setup. The LCS (left) scans a meteorite presented on a turntable (right) at a distance of 1.2 m.

Camera-target distance	m	1.2
Field of view	degree	30 x 30
Image resolution	voxel	512 x 512
Integration time	µs	180
No. of scans per meteorite	-	9 - 12

Table 1.2. Characteristics of the 3D laser images acquired in this study.

1.1.3 *Assembling 3D Images into Volumetric Models*

The 3D laser images were processed using Polyworks, a 3D visualization software developed by InnovMetric of Quebec City, Canada (http://www.innovmetric.com). Polyworks merges individual scans into a detailed volumetric closed model. Polyworks was initially designed for reverse-engineering applications in the automotive industry, and has gradually gained acceptance in art and archeology for the virtual preservation of artifacts. In this study and its precursors (Herd et al. 2003; Smith et al. 2005a, 2005b, 2005c), the process is applied for the first time to rock material. It is illustrated in Figs. 1.3 to 1.7 for the Blithfield meteorite.

First, at the file importing stage, the point cloud data (Fig. 1.3) of each individual scan are interpolated and converted into a mesh composed of many triangles (Fig. 1.4). The number of triangles depends on the topology of the target surface. A smooth surface will be represented by a few large triangles whereas several small triangles are necessary to fit an edge or rough topology.

Second, individual meshes are aligned one at a time. The user imports two adjacent meshes (Fig. 1.5) and the software performs a best-fit alignment (Figs. 1.6a, 1.6b). Meshes are progressively added until a closed volumetric model is formed. Two criteria must be met for successful alignment: each mesh must share redundant information with adjacent meshes and each mesh should contain at least one change of shape (e.g. corner, hole, edge). This last criterion, easily met for industrial parts, was more challenging to meet for meteorites which have mostly semi-rounded features. Finally, the model is checked for topology "water tightness" and any remaining holes in the data are filled. The software can then compute the enclosed volume automatically. The mass of the fragment being already available in the database of the National Meteorite Collection of Canada, the bulk density of the meteorite can be easily

determined by dividing mass by volume and the images can be stored for future investigations. Appendix IV contains the eleven stony meteorite models used in the present study. These files have been archived for future use (.stl, .obj, and .pol formats) and may be accessed via compact disc.

The final volumetric model of the Blithfield meteorite is shown in Fig. 1.7. The model can be compared directly to a digital picture of the meteorite (Fig. 1.8), attesting to the fidelity of the 3D laser imaging technique. Assembling 3D images into volumetric models using Polyworks takes approximately 45-60 minutes per meteorite and requires a user with proficient skill and knowledge of the program. Thus, coupled with the time required for data acquisition, the bulk density of any fragile, soluble or porous object can be determined without contamination or degradation of the sample within 90 minutes.

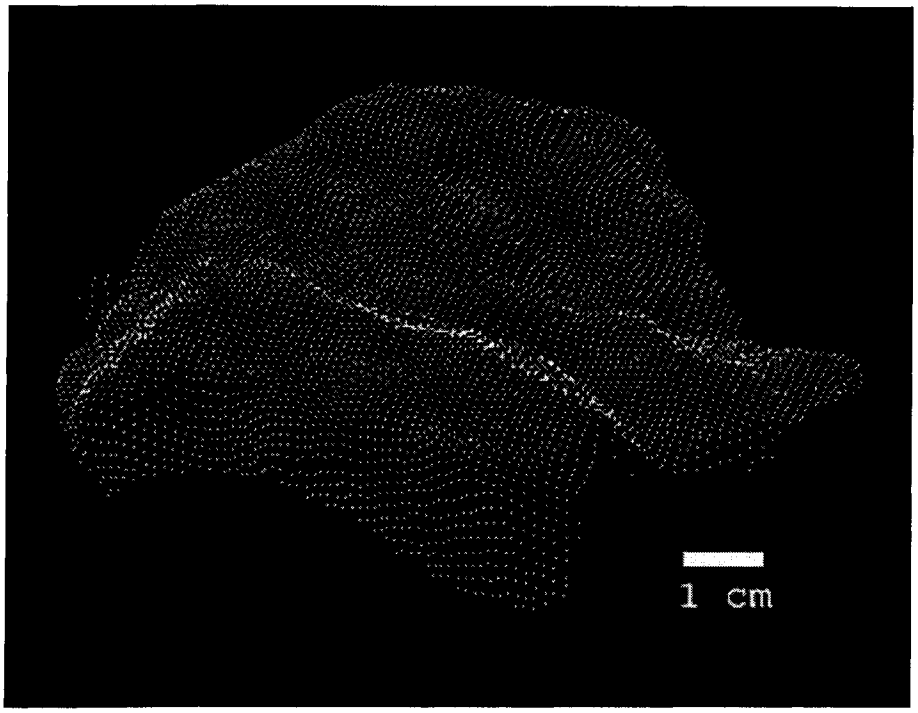

Fig. 1.3. Point cloud data for one individual scan of the Blithfield meteorite.

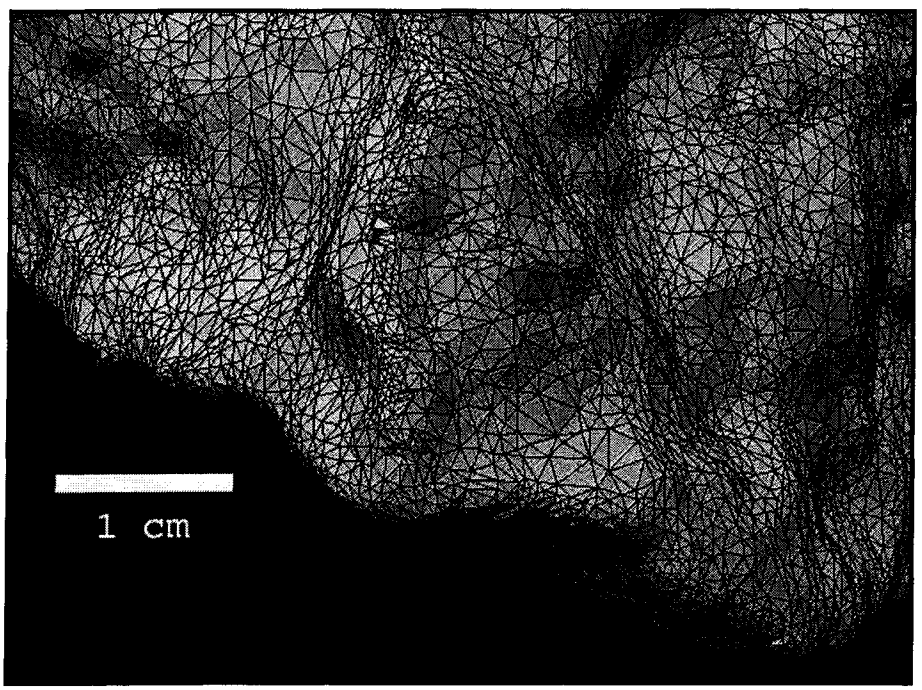

Fig. 1.4. A meshed view of the Blithfield meteorite. Triangles displayed.

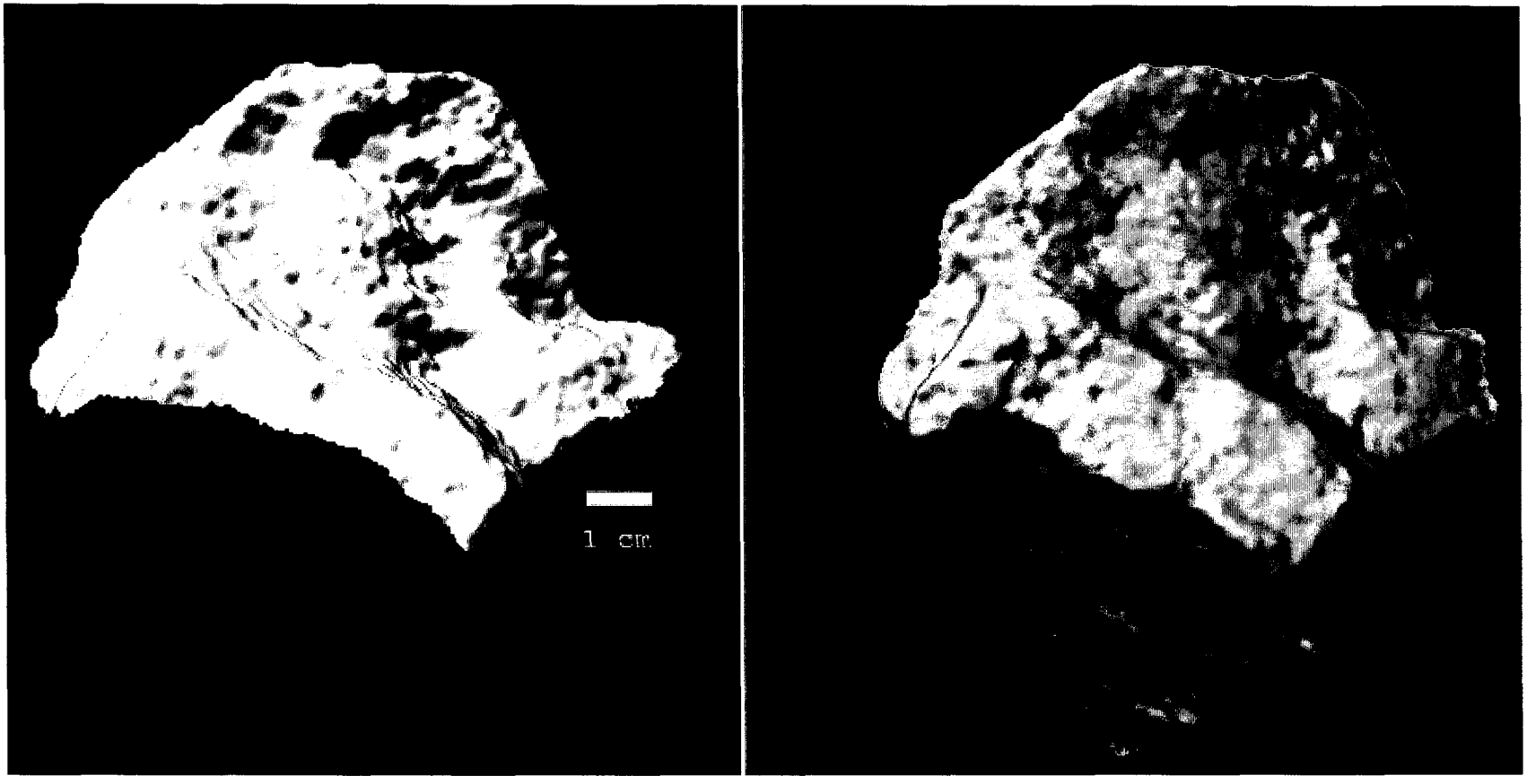

Fig. 1.5. Two meshed views of the Blithfield meteorite before alignment. Different colours represent data from different scans.

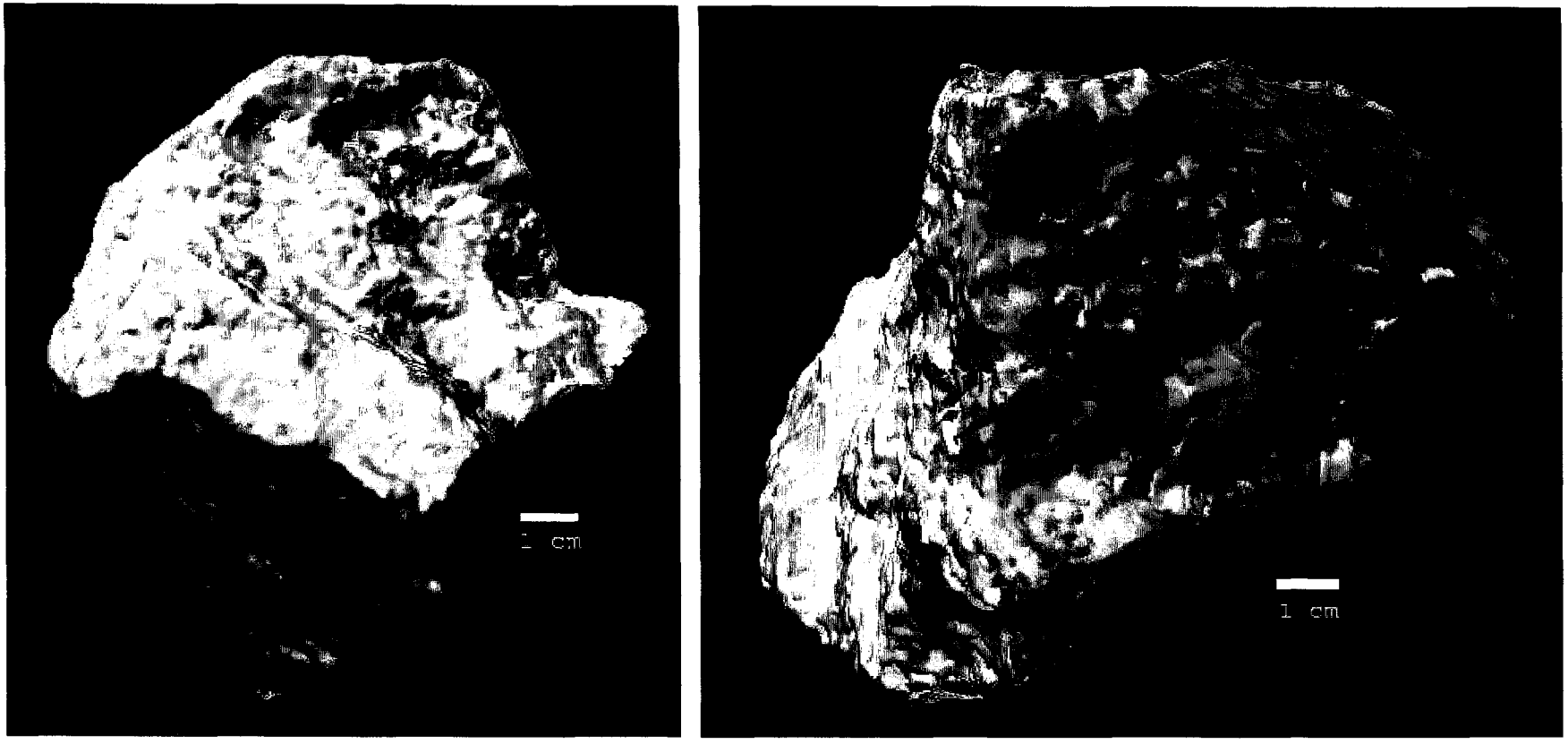

Fig. 1.6. (a) Two and (b) three meshes of the Blithfield meteorite after alignment. Different colours represent data from different scans.

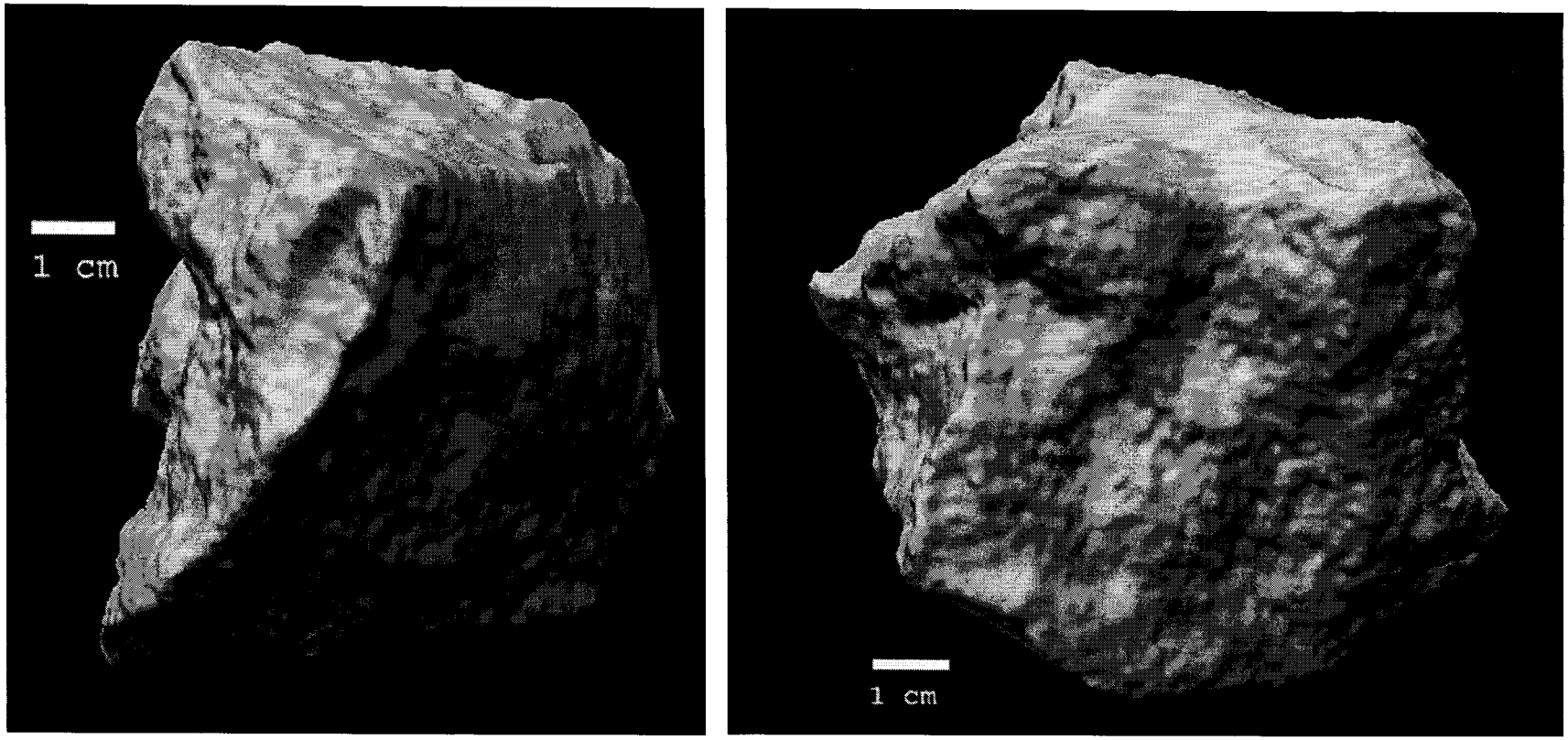

Fig. 1.7. Two views of the volumetric model of the Blithfield meteorite.

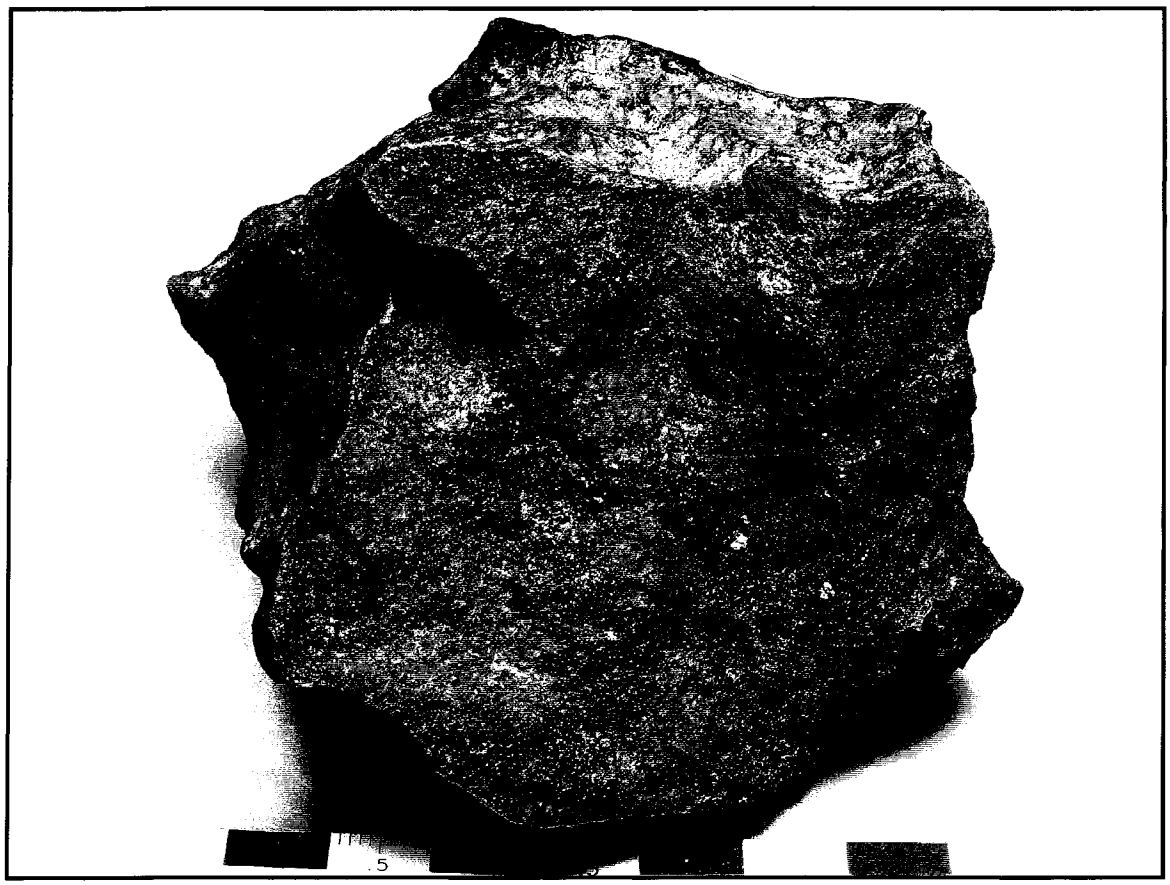

Fig. 1.8. Digital picture of the Blithfield meteorite (each black/white block corresponds to 1 cm). (Photo courtesy R. K. Herd)

1.1.4 *Error Analysis*

A test was performed to compare volume estimates derived from Archimedes' Principle and 3D laser imaging (J-E Sink 2005, Neptec internal report, pers. comm.). Both methods were tested using three limestone hand samples of different size and shape. Results are shown in Table 1.3. Differences between the measurements of the two methods are 2.7 % or less. The difference is smallest for samples 1 and 2 suggesting that there may be slightly less error associated with objects of larger volume.

For several meteorites, the process of assembling 3D images into volumetric models described in Section 1.1.3 was repeated in order to test the precision of the approach. Although adjacent meshes were aligned in a different order, the precision was consistently better than 1%.

In four cases, the precision was also determined using two fragments of the same meteorite of different size and shape. Bulk densities should be the same assuming no veining or heterogeneities between fragments. Bruderheim was the best candidate for this test as veining has not been observed in this meteorite. The difference between the two Bruderheim fragments was less than 1% (Table 1.4). The densities of the two Mocs meteorite fragments show the largest difference. This may be attributed to the presence of inconsistent veining between the two fragments. Pultusk is a veined breccia. The densities of the two Pultusk fragments, however, are very close suggesting minimal or consistent veining for the fragments measured.

	Volume [cm^3]		Difference between methods [%]
	Archimedes' Principle	3D Laser imaging	
Sample #1			
Trial 1	99.0	100.7	1.8%
Trial 2	99.0	101.5	2.5%
Sample #2			
Trial 1	109.0	111.0	1.9%
Sample #3			
Trial 1	20.0	19.5	-2.7%
Trial 2	20.0	19.5	-2.7%

Table 1.3. Comparison between volume measurements derived from Archimede's Principle and 3D laser imaging (a negative difference value means that the volume derived from Archimede's Principle is larger).

Meteorite				Bulk Density [g/cm^3]			Difference between 3D Laser imaging and Britt and Consolmagno [%]
Name	Class	Find/Fall	Mass [g]	3D Laser imaging	Britt and Consolmagno (2003)	Wilkison[g] (2003)	
Allende	CV3.2	Fall	754.00	2.97	2.88±0.05[a,g,c,s]	-	3.1
Allende	CV3.2	Fall	492.00	3.00	2.88±0.05[a,g,c,s]	-	4.1
Pultusk	H5	Fall	276.00	3.57	3.47±0.05[a,g]	3.60±0.08, 3.54±0.04, 3.56±0.04	3.0
Pultusk	H5	Fall	45.36	3.60	3.47±0.05[a,g]		3.7
Blithfield	EL6	Find	625.60	3.93	-	-	-
Bruderheim	L6	Fall	277.50	3.43	3.34±0.04[a,g,c,s]	-	2.7
Bruderheim	L6	Fall	122.80	3.46	3.34±0.04[a,g,c,s]	-	3.5
Mocs	L6	Fall	29.87	3.30	3.18±0.08[a,g]	3.25±0.03	3.7
Mocs	L6	Fall	151.00	3.35	3.18±0.08[a,g]		5.2
Millbillillie	EUC	Fall	55.98	2.82	2.86[g]	-	-1.3
Norton County	AUB	Fall	32.38	2.87	2.97±0.12[a]	-	-3.3

Table 1.4. Meteorite bulk densities (a negative difference value means that the density determined using 3D laser imaging is smaller). Mass data extracted from the National Meteorite Collection of Canada database.
[a] Archimedes' method (various liquids)
[g] Glass bead method
[c] Clay molding
[s] Shaping meteorite into basic shape for volume measuring

1.2 Results and Discussion

Bulk density values of eleven chondrites and achondrites determined using 3D laser imaging are listed in Table 1.4. These densities compare very well with previously published values. Note that the densities published in Wilkison et al. (2003) are all based on the glass bead method, whereas the densities published in Britt and Consolmagno (2003) have been derived by a variety of methods. The average difference between the densities determined using 3D laser imaging and the densities published in Britt and Consolmagno (2003) is 3.4%.

The difference between densities determined using 3D laser imaging and previously published values may be attributed to (1) the presence of heterogeneities and (2) the limited amount of comparative data available. Heterogeneities may be a result of inconsistent veining or brecciation producing unevenly distributed clasts of variable size. Heterogeneities may partially explain the observed differences for the Pultusk (veined breccia), Millbillillie (polymict breccia) and Mocs (veined) meteorites. Meteorite density data in the literature are scarce and thus most meteorites have not had more than one fragment measured. When more than one fragment has been measured it might not have been by the same technique. This significantly limits generalization of the results obtained.

For nine out of the eleven samples studied, the densities determined using 3D laser imaging are higher than previously published values. The nature of the method used for determining the volume of the meteorite may have introduced measurement biases. For example, all Archimedean methods suffer from the wall effect where the friction between the fluid and the container creates a concave fluid-air interface. In the Archimedean glass bead method, there is also unavoidable space left between the beads. Both the wall effect and the finite size of the beads lead to an overestimation of the measured

volume and thus to a lower estimation of the density. Laser imaging does not suffer from these experimental errors and may provide a more reliable measurement of volume.

Millbillillie (glass bead method) and Norton County (Archimedean fluid method) are the only meteorites for which the densities determined using 3D laser imaging are lower than previously published values. In the case of Millbillillie, the difference is only -1.3 %. Its density, however, determined using the glass bead method, has been measured on only two fragments limiting the statistical reliability of a comparison. Moreover, Millbillillie is also brecciated which may cause variability among fragments.

Norton County has a larger difference of -3.3%. Apart from random heterogeneities between fragments of the same meteorite, the most plausible explanation for the difference is in the measurement technique. Norton County physically stands out among the other ten meteorites due to its lighter appearance, rough exterior and highly fragile nature (Fig. 1.9). Britt and Consolmagno (2003) list two measurements of Norton County; both measured using water displacement (Archimedes method). However, the relatively high porosity of Norton County (~ 11%) may have biased the measurements as some fluid may have leaked into the pore spaces along cracks and between grains. This would cause an underestimation of the volume of the meteorite and a corresponding overestimation of its bulk density. On the other hand, Norton County has many sharp corners and edges which may have caused appreciable shadow effects while scanning with the LCS. This effect would lead to an overestimation of the volume and a corresponding underestimation of bulk density. Combined, the unique roughness and porosity of Norton County may explain the difference between the bulk densities derived from Archimedes' Principle and 3D laser imaging.

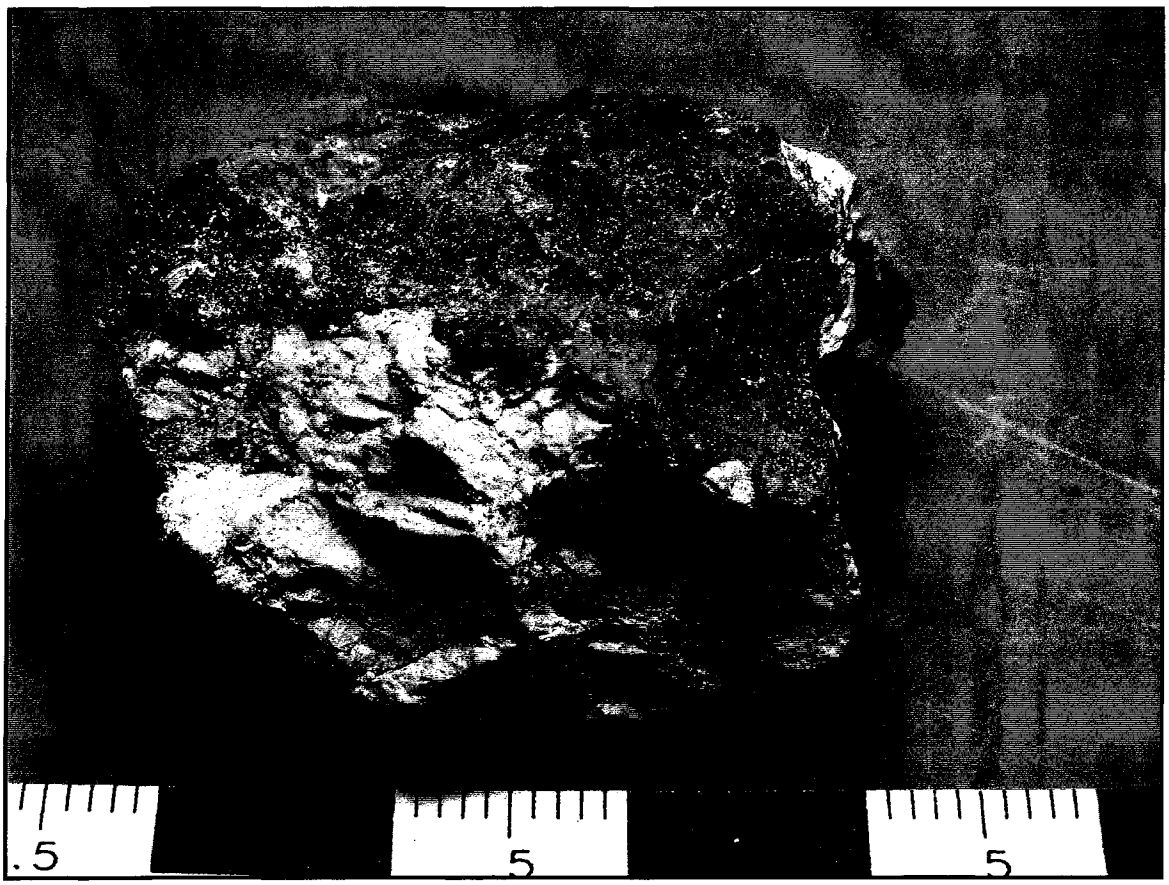

Fig. 1.9. Digital picture of the Norton County meteorite (each black/white block corresponds to 1 cm). Note the lighter appearance and rough exterior. (Photo courtesy R. K. Herd)

Chapter I (Part II)

A Semi-quantitative Pilot Approach for Description of Meteorite Surface Roughness

1.3 Introduction

Over 25,000 meteorites have been discovered on Earth to date, each providing clues about the processes that formed them and the solar nebula from which they were derived. A variety of characterization techniques are currently in use in an effort to elucidate the information stored in them (e.g. magnetism, chemical analysis, petrophysics, etc.) (e.g. Jarosewich 1990; Terho et al. 1993; Genge and Grady 1999). One physical characteristic that varies among meteorites and has not generally been explored in past studies is surface roughness. For most meteorites a fusion crust covers the entire surface unless weathering or other processes has removed a portion of it, revealing the underlying mineral constituents. The internal mineralogy of the meteorite governs the composition and development of the fusion crust (Genge and Grady 1999) and as mineralogy varies among meteorites so will its surface properties, crust present or not. Therefore surface roughness might be a useful additional parameter to measure for meteorite characterization.

Surface roughness can be estimated qualitatively by naked-eye visual inspection and touch. The present study investigates a more rigorous, semi-quantitative approach of surface roughness estimation based on 3D laser image data. A pilot approach has been used to study the eleven stony meteorite fragments previously used for density determination.

1.4 Methodology and Approach

In this study, the same 3D models built to determine the volume of meteorites (Smith et al. 2005d) have been used to analyze meteorite surface roughness by varying the tolerance and relating this change to file compression in the Polyworks visualization software.

As mentioned earlier, each Polyworks 3D model is built of many triangles. The triangles' relative position and size are determined by the tolerance used to interpolate the point cloud data during the polygonalization process. Tolerance *T* is defined as the maximum distance between points that form a single triangle. Polyworks will include all points within this distance into the same triangle using a best fit algorithm; correspondingly, any point falling outside will form a new triangle and connect with adjacent triangles. As tolerance is increased, the number of triangles decreases and the size of the computer file describing the model decreases. The magnitude of this file compression is calculated as follows and expressed as a percent.

[1.1] File Compression [%] = (Initial File Size - Final File Size) / (Initial File Size) x 100

where the initial file size is the size when the tolerance is equal to zero. The 3D model of Norton County is used to illustrate the decrease in the number of triangles as tolerance increases (Figs. 1.10 to 1.13). The number of triangles alone cannot be used as a direct measure of surface roughness as the eleven meteorites are not equal in size.

For a given tolerance, the rougher the meteorite surface, the smaller the file compression percentage should be as many triangles are required to fit the irregular topology. File compression is therefore an indirect estimate of surface roughness. To test this hypothesis, a file compression analysis was repeated at three different

tolerances (0.10, 0.25 and 0.50 mm) and applied to all meteorite fragments imaged with the LCS. The technique is semi-quantitative as only a relative comparison between the meteorites is achieved. The results of the analysis are compared to a qualitative naked-eye visual inspection of the meteorites where the surface roughness index 1 has been attributed to smooth surfaces, 2 to irregular surfaces and 3 to very rough surfaces.

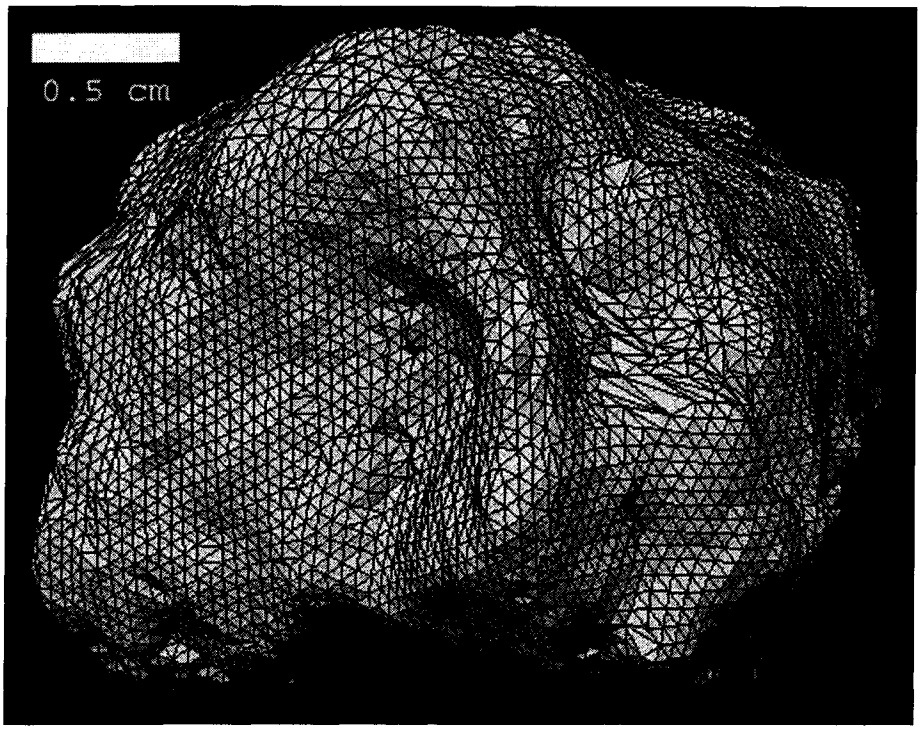

Fig. 1.10. Norton County: Initial tolerance = 0.00 mm.

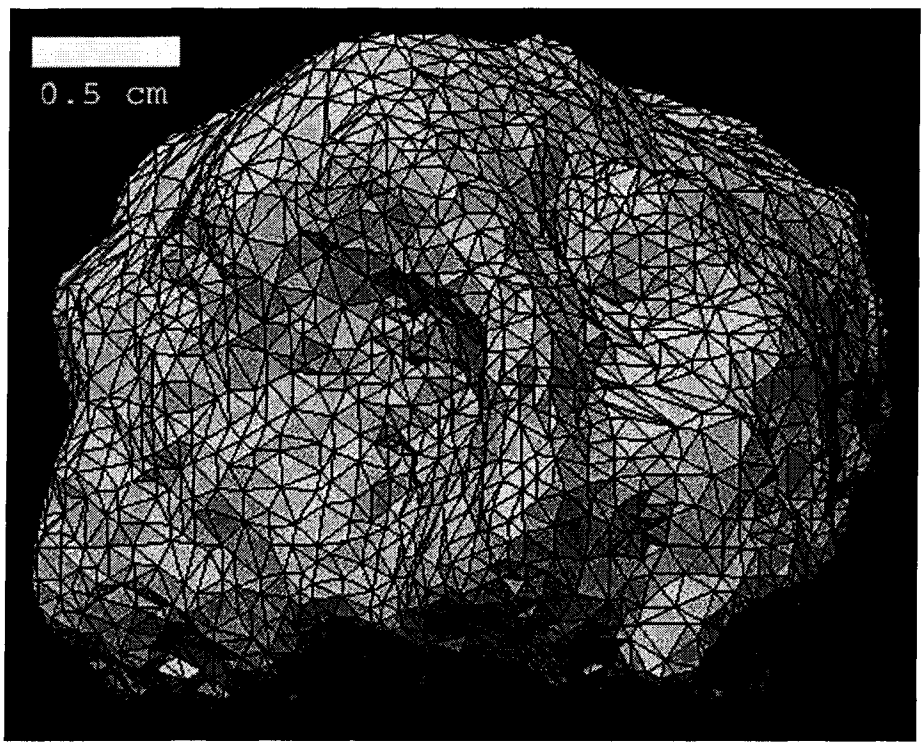

Fig. 1.11. Norton County: Tolerance = 0.10 mm.

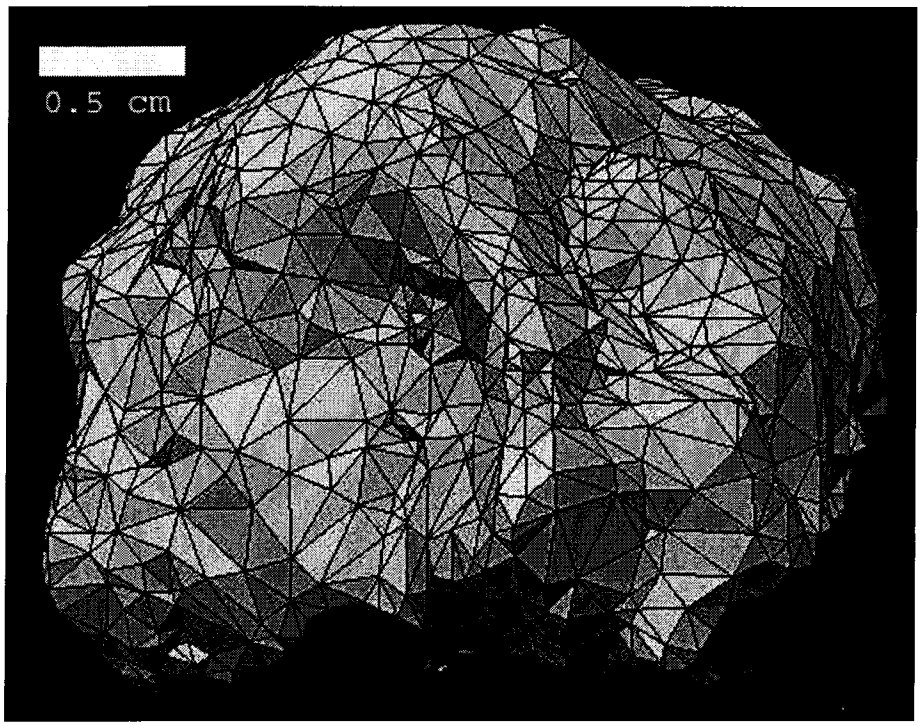

Fig. 1.12. Norton County: Tolerance = 0.25 mm.

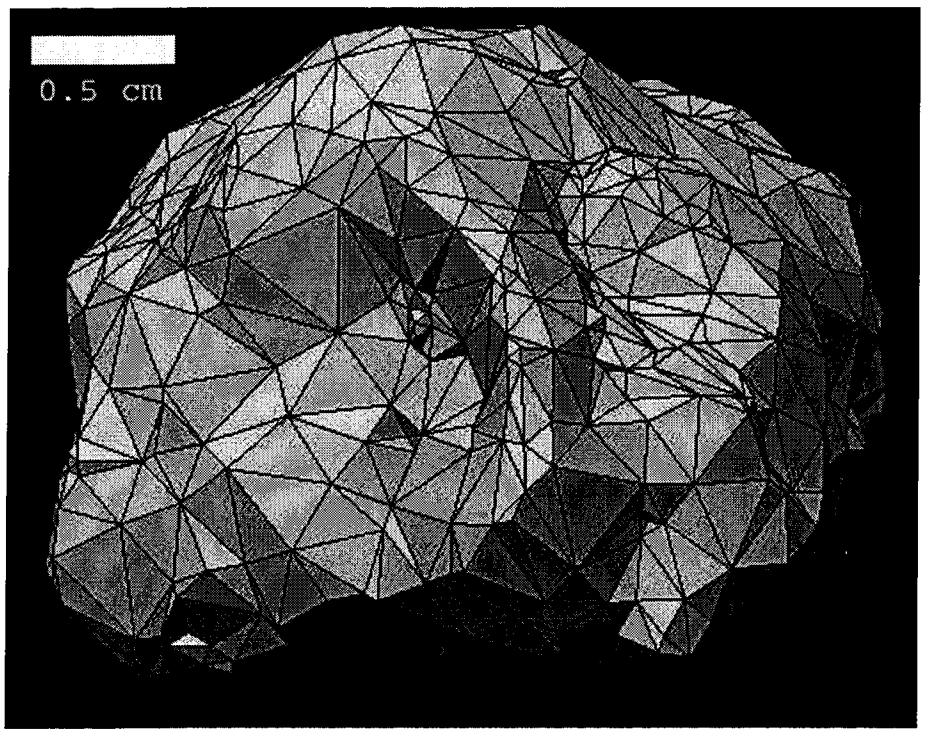

Fig. 1.13. Norton County: Tolerance = 0.50 mm.

1.5 Results and Discussion

Results are presented in Fig. 1.14 and Table 1.5. As expected, the general trend is that meteorites with irregular and rough surfaces (indices = 2 or 3) show the least amount of file compression. This trend is observed for all three tolerance values. Initial file size does not appear to significantly influence file compression as seen from the varied compression percentages of the smaller meteorite fragments.

Visually Norton County has the roughest surface due to its lack of crust exposing its fragile interior. Correspondingly, Norton County has the smallest compression percentage at all three tolerances. The largest Pultusk (276 g) and Mocs (151 g) meteorites are visually among the smoothest of all the meteorites and have the highest compression percentage. Millbillillie is entirely covered by a fusion crust. Visually, however, its surface is not as smooth as that of the other meteorites. Many small ridges and crevasses are present. These characteristics are reflected in the smaller compression percentage for that meteorite. Blithfield also has a visually rougher exterior than most; it shows a mid to low range of file compression comparatively.

Of the eleven meteorites fragments evaluated, Norton County and Millbillillie are achondrites and both display the least amount of file compression, that is, a greater roughness than the others. This may be due to the markedly different mineralogy of achondrites compared to chondrites. However, it may also be coincidental as too few meteorites have been evaluated, limiting the statistical viability of the analysis. Furthermore, the surface of Millbillillie is entirely covered by a fusion crust whereas only about a quarter of the surface of Norton County is covered by a fusion crust, making comparison difficult. Crust is typically different in texture than the interior of a meteorite and this may significantly influence estimates of the overall surface roughness. Thus, in future studies, an attempt should be made to select meteorites with either 100% or 0%

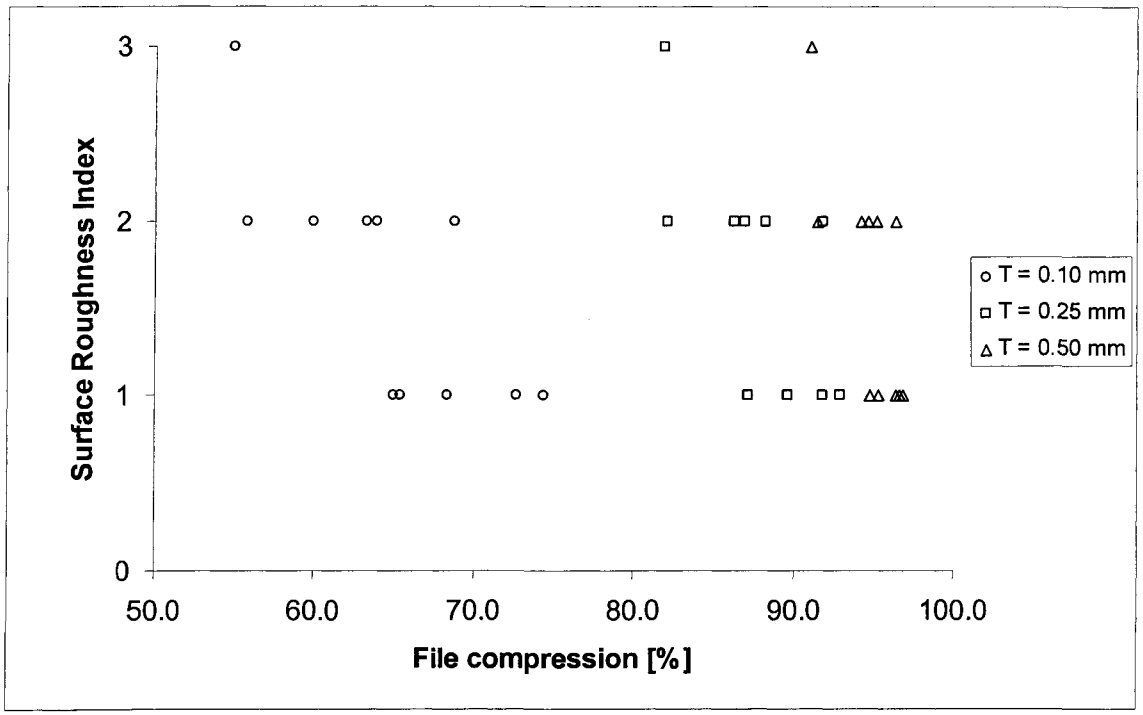

Fig. 1.14. Surface roughness index versus percentage of file compression.

Meteorite		Surface roughness index from visual inspection	Initial File Size [kb]	File Compression [%]		
Name	Mass [g]			T=0.10 [mm]	T=0.25 [mm]	T=0.50 [mm]
Allende	754.00	2	4651	60.0	86.4	95.2
Allende	492.00	2	3766	68.8	91.9	96.4
Pultusk	276.00	1	3444	72.7	91.8	96.6
Pultusk	45.36	1	992	68.3	89.7	95.4
Blithfield	625.6	2	3797	63.3	87.0	94.3
Bruderheim	277.50	1	2409	65.5	89.7	96.5
Bruderheim	122.80	2	1275	63.9	88.3	94.7
Mocs	29.87	1	503	65.0	87.3	94.8
Mocs	151.00	1	2518	74.4	92.9	96.9
Millbillillie	55.98	2	862	55.8	82.1	91.5
Norton County	32.38	3	566	54.9	82.0	91.2

Table 1.5. Results of meteorite surface roughness analysis. An index of 1 is attributed to smooth surfaces, 2 to irregular surfaces and 3 to very rough surfaces. Mass data extracted from the National Meteorite Collection of Canada database.

fusion crust present. Such a distinction could not be made in the present study as the meteorites had been selected primarily for density analysis in Smith et al. (2005d).

The difference in file compression percentages among fragments of the same meteorite can be partially attributed to the extent of fusion crust on each fragment, as is likely the case for Allende. On the other hand, the two Mocs fragments have similar extents of fusion crust present but rather different compression percentages. The smaller Mocs meteorite, however, appears to have suffered more severe weathering altering its exterior. This is the most plausible cause of the difference in surface roughness between the two Mocs fragments.

The spread of data points along the horizontal "File compression [%]" axis in Figure 1.14 might reflect the size distribution of surface irregularities. In most cases, compression percentage increases are larger as tolerance increases from 0.10 to 0.25, than when it increases from 0.25 to 0.50 mm. This would indicate that there is a larger number of surface irregularities of size < 0.25 mm than > 0.25 mm. The effects of large-scale surface features like edges and topographical depressions and highs on the results are not clear.

This pilot study has investigated one method of surface roughness description using existing Polyworks image data. Along with refining the current approach, other computational methods including dividing the surface area by number of triangles and fractal techniques may prove useful.

Chapter II

Stony Meteorite Characterization by Non-Destructive Measurement of Magnetic Properties*

2.0 Introduction

The large and increasing number of meteorites being found in Antarctica, and in deserts in Asia and Africa, has resulted in a backlog of unclassified meteorite specimens. Some of these meteorites are unique and small, and their characterization and preservation for further study is a priority, especially if they prove to be rare. There exists a need for rapid, accurate and non-destructive classification, to distinguish rare from common types and chondrites from achondrites.

Magnetic properties such as natural remanent magnetisation (NRM) have been used as the basis of past meteorite classification (e.g. Sugiura 1977); however, overprints of secondary magnetizations unrelated to the remanence of the parent body make characterization difficult. Other traditional methods (e.g. visual inspection, magnetic hysteresis, chemical analysis) are time consuming, destroy the paleomagnetic signal or require the meteorite to be reduced in size (i.e. fragmented) for analysis (Jarosewich 1990; Rochette et al. 2001).

Earlier work by Kukkonen and Pesonen (1983), Rochette and co-workers (2001, 2003) and Smith (2003) investigated the use of low field bulk magnetic susceptibility as a method of classification of stony meteorites. Their technique essentially measured the amount of Fe-Ni metal and Fe-Ni sulphide within the sample. As metal content is the

*Chapter II material is adapted from Smith et al. (2005a)

basis of current meteorite classification, bulk magnetic susceptibility provides an efficient means of rapid classification. Due to differing magnetic mineral abundances and compositions, the inherent magnetic susceptibility of meteorites is generally outside the range of terrestrial rocks (Kukkonen and Pesonen 1983). The main magnetic constituents of terrestrial rocks are iron and titanium oxides; those of meteorites are iron-nickel alloys, mainly kamacite and taenite with oxides dominant at times (Nagata 1979; Dunlop and Ozdemir 1997). Therefore, magnetic susceptibility is an effective and very important means of distinguishing these materials, as stony meteorites may be difficult to easily recognize in the terrestrial environment by other tests.

In the present study, non-destructive measurement of stony meteorite magnetic properties has been systematically undertaken to: (1) define a range of properties for each chondritic and achondritic class; (2) develop simple techniques to discriminate among classes and within classes, and (3) gain insights into the conditions under which meteorites formed, and therefore into the nature and history of their parent bodies.

Four parameters showing promise as classification tools and discriminants have been evaluated: (1) bulk magnetic susceptibility (MS), (2) its frequency dependence, and (3, 4) the degree and shape of the anisotropy of magnetic susceptibility (AMS). Previously published bulk susceptibility measurement techniques (Rochette et al. 2001, 2003) have been extended to include measurements at two different frequencies (825 and 19000 Hz) (Appendices I, II, III). Bulk susceptibility measurements were performed on 321 specimens at both frequencies to yield parameters (1) and (2). In addition, 145 of these 321 specimens, covering 14 classes of chondrites, primitive achondrites and achondrites, have also been measured for AMS at a frequency of 19000 Hz yielding parameters (3) and (4) (Smith et al. 2004). Until very recently, only a handful of published studies has been done involving AMS measurements on several dozen meteorites; they all focused, however on LL, L, H, E and C chondrites, and involved no

other classes (e.g. Martin and Mills 1980; Hamano and Yomogida 1981; Sugiura and Strangway 1983; Sneyd et al. 1988; Morden and Collinson 1992). Recently, Gattacceca et al. (2005) investigated the AMS of LL, L, C and R chondrites and HED and SNC achondrites. This study and that of Gattacceca et al. (2005), present the most comprehensive studies of meteorite AMS to date.

All the specimens used in this study belong to the National Meteorite Collection of Canada of the Geological Survey of Canada (GSC), Natural Resources Canada. The collection contains approximately 2700 meteorite specimens belonging to 1100 different meteorites. Among these are 730 different stony meteorites. This Canadian collection thus represents an exceptional opportunity to further apply and expand the magnetic susceptibility approach recently advocated by Rochette and co-workers (2001, 2003). The present study concentrates on stony meteorites. Measurements on stony iron and iron meteorites require different instrumentation due to their high metal content.

2.1 Methodology

Bulk magnetic susceptibility (MS) was determined at two different frequencies (825 and 19000 Hz) on a SI-2B instrument manufactured by Sapphire Instruments of Ruthven, Ontario (Fig. 2.1). The SI-2B instrument is comprised of a built-in internal coil and of an external coil attached to it. The 4.5 cm diameter internal coil operates at 19000 Hz and the 5.1 cm diameter external coil operates at 825 Hz. Both coils operate using the same field geometry and applied magnetic field strength of 24 A/m (M. Stupavsky 2005, Ruthven, ON, designer of the SI-2B, pers. comm.).

Magnetic susceptibility measurements were performed by placing the meteorite into the magnetic field generated by either coil and recording the intensity of

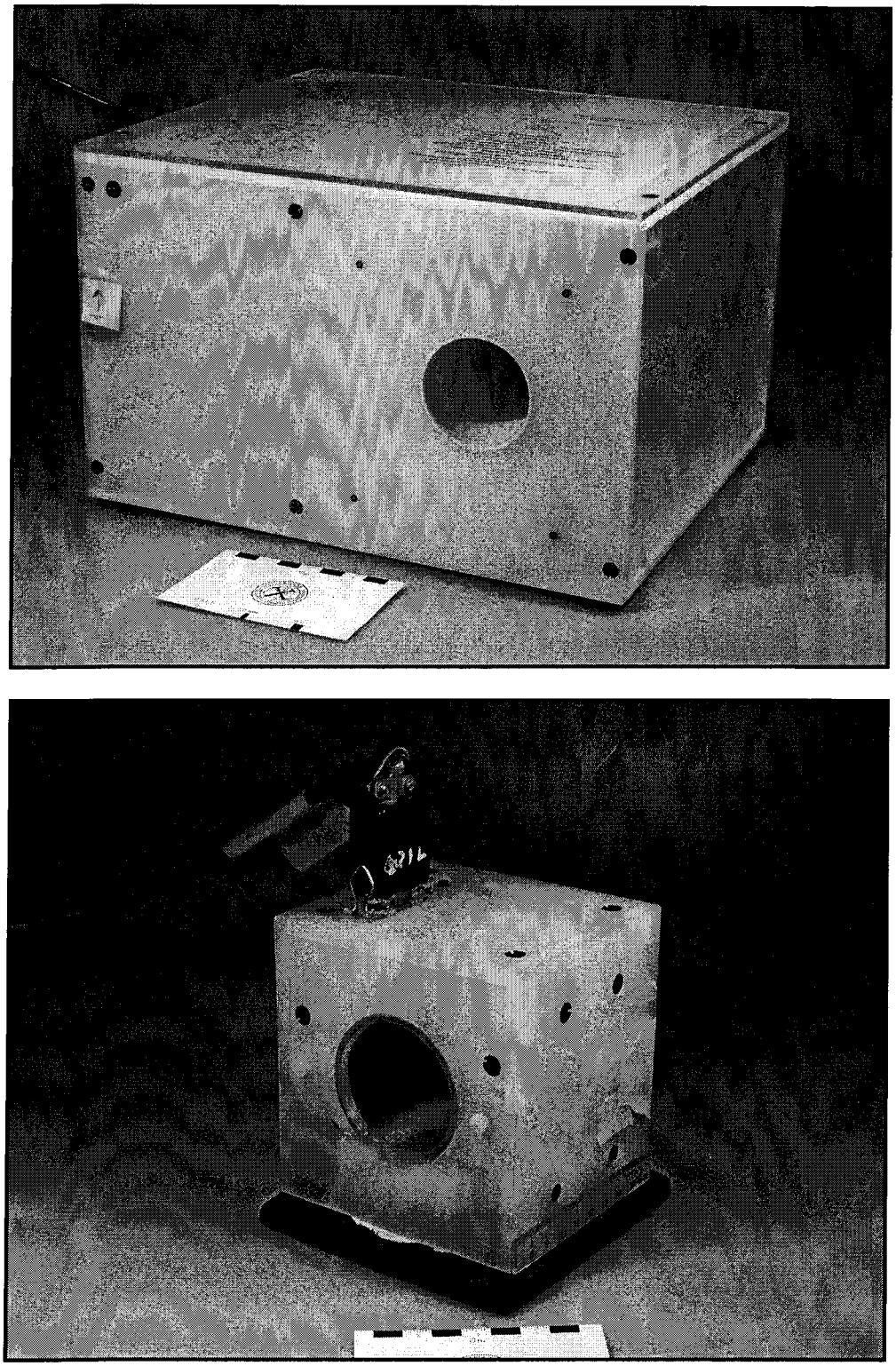

Fig. 2.1. SI-2B instrument manufactured by Sapphire Instruments. Internal coil (top) and external coil (bottom). (Photo courtesy R. K. Herd)

magnetization induced within the sample. A single measurement took less than one minute to complete. Five measurements were made for each frequency with the average being reported and used for further analysis. For each specimen multiple measurements were made in different orientations to reduce the effects of AMS (referred to as 'random orientation' method). A full AMS was not possible for all specimens because of size constraints imposed by the measurement coil. Specimens were centred in each coil for each measurement.

The frequency dependence of magnetic susceptibility was evaluated using the above described procedure for both of the frequencies. This method gave reproducible MS results to within <1-3% of the mean over five sets of measurements. The reliability of this "random orientation" method was validated by comparing it with another method whereby exactly the same axis of the specimen is measured at the two frequencies. The data are presented in Table 2.1.

The specimen masses ranged from 0.12 -143 g. The internal coil (19000 Hz) has a greater precision, but the external coil (825 Hz) was necessary to accommodate larger specimens. Coil saturation at 19000 Hz was reached for several specimens, but in such cases, values were still obtainable on the external 825 Hz coil.

AMS measurements were performed at 19000 Hz using a 6 orientation analysis to define the susceptibility ellipsoid from which values for both degree and shape of anisotropy were calculated. Specimens were wrapped in plastic cling wrap and placed in a diamagnetic sample holder, which was then stuffed with tissue to ensure no movement of the specimen during the analysis. Approximately ten minutes were required for each full analysis. The mass of each specimen ranged from 0.12 -18.44 g. The size of the sample holder, a cylinder of 2.4 cm diameter and 2.4 cm length, limited the size of the specimen.

Meteorite	K 19000 Hz ($x10^{-6}$ SI)	K 825 Hz ($x10^{-6}$ SI)	K_{FD} (%)
Chassigny (random orientation)	272	278	2.1
Chassigny (same axis)	275	280	1.7
Shergotty (random orientation)	122	134	9.6
Shergotty (same axis)	117	127	9.0
Zagami (random orientation)	473	488	3.2
Zagami (same axis)	478	492	3.0
ABEE (random orientation)	980662	996101	1.6
ABEE (same axis)	1107942	1130581	2.0
ABEE matrix (random orientation)	367211	390817	6.4
ABEE matrix (same axis)	384201	406091	5.7
Roosevelt County 070 (random orientation)	832	850	2.2
Roosevelt County 070 (same axis)	856	876	2.3
NWA 725 (random orientation)	123933	155639	25.6
NWA 725 (same axis)	108457	132445	22.1

Table 2.1. Measurement methods of frequency dependence. Comparison of magnetic susceptibility values (K in SI [Système International] units) using the random orientation method described in Section 2.1 and the same axis method. Values for both frequencies are normalized using a 19g MnO_2 standard. K_{FD} (%) = χ_{FD} (%) (See equation [2.3]). K is a dimensionless quantity measured using an assumed volume of 11 cm^3.

2.1.1 *Calculations*

For each specimen, the bulk mass magnetic susceptibility χ was calculated rather than the bulk volume magnetic susceptibility K for two reasons: (1) it is easier to determine the mass of an irregularly shaped meteorite than its volume; and (2) to maintain consistency with the previously published databases of Rochette et al. (2001, 2003) where χ is reported. To obtain values of χ, the readings of the SI-2B instrument had to be divided by the density of the specimen. Bulk mass magnetic susceptibility χ (m^3/kg) can be expressed as:

$$[2.1] \quad \chi = K/\rho = KV/M = V\,(K_{=11}\,(V_s/V)/M) = K_{=11}V_s/M,$$

where K is the reading of the SI-2B instrument in SI units, and ρ (kg/m^3) the density, V (m^3) the volume and M (kg) the mass of the specimen. A standard volume (V_s) of 11 cm^3 was used for each specimen; correspondingly, $K_{=11}$ is the output of the SI-2B instrument using the standard volume. Both $K_{=11}$ and V_s were required as the specimen volume is unknown. This standard volume was of the order of the volumes for all specimens measured with only a few exceptions. The mass was already known for each specimen from the database of the National Meteorite Collection of Canada. Because the bulk mass susceptibility values ranged over four orders of magnitude, the same procedure as in Rochette et al. (2001) was followed and the decimal logarithm of χ expressed in 10^{-9} m^3/kg was reported. This narrowed the range of values to between 2 and 6.

The SI-2B instrument is temperature sensitive; therefore all measurements were taken at room temperature. At the beginning of each session, measurements on a sample standard composed of fine-grained MnO_2 were also used to correct for minor day-to-day variations in room temperature. Data for the two frequencies were also

normalized to the same MnO_2 value ($K=569x10^{-6}SI$), as MnO_2 is paramagnetic and non-conducting at room temperature and therefore should not display a frequency dependence (Ellwood et al. 1993; A. M. Hirt 2004, Zurich, Switzerland, pers. comm.).

The average $\log\chi$ for multiple specimens of the same meteorite were computed using two approaches. In the first approach (Table 2.2, third column), bulk mass susceptibility values are computed using the summed masses and bulk volume magnetic susceptibilities of all the specimens in the following manner:

$$[2.2] \quad {}^{1\text{-}3}\chi = V_s ({}^1K_{=11} + {}^2K_{=11} + {}^3K_{=11}) / ({}^1M + {}^2M + {}^3M).$$

In the second approach (Table 2.2, fourth column), each specimen was assigned equal weight in computing the average for a specific meteorite. This approach, however, may introduce significant error for specimens that have a small mass and an extensive fusion crust (see section 2.2). The first method is therefore a more accurate representation of the meteorites true bulk mass susceptibility.

Mean bulk mass MS and AMS measurements for each meteorite class were calculated and presented giving equal weight to each meteorite in their respective classes by first calculating the mean of a meteorite with multiple specimens and then using this value in the class mean (Table 2.3).

Frequency dependence of bulk magnetic susceptibility in percent, $\chi_{FD}\%$, was calculated using the equation:

$$[2.3] \quad \chi_{FD}\% = | 100 * (\chi_{825} - \chi_{19000}) / \chi_{19000} |,$$

where χ_{825} and χ_{19000} are the bulk mass magnetic susceptibility in SI units at 825 and 19000 Hz, respectively. This equation follows closely the formulation of Dearing et al. (1996) and Worm (1998); however, the higher frequency (19000 Hz) data were used here for normalization as that coil has the lowest detection limit.

Meteorite	Class	Logχ 19000 Hz*	Logχ 19000 Hz
ABEE	EH	5.45	5.46±0.04 (3)
Bishopville	AUB	3.07	3.05 (2)
Bruderheim	L6	4.91	4.91±0.08 (7)
Camel Donga	EUC	4.32	4.26±0.20 (12)
Cold Bokkeveld	CM2	3.49	3.56±0.20 (3)
Coolidge	C3.8-4 UNGR	4.90	4.90 (2)
Daniel's Kuil	EL6	5.62	5.28±0.64 (3)
Forest City	H5	5.28	5.27 (2)
Happy Canyon	EL	4.34	4.00 (2)
Hessle	H5	5.21	5.19 (2)
Indarch	EH4	5.39	5.39±0.06 (5)
Johnstown	DIO	3.43	3.50 (2)
Kenna	URE	4.56	4.55 (2)
Knyahinya	L/LL5	4.68	4.67 (2)
La Criolla	L6	4.74	4.78±0.06 (3)
Leoville	CV3.0	4.56	4.51 (2)
Millbillillie	EUC	2.66	2.67±0.06 (49)
Mulga (north)	H6	5.07	5.07±0.10 (4)
Murchison	CM2	3.61	3.69 (2)
Nakhla	SNC	3.23	3.26 (2)
Norton County	AUB	3.30	3.37±0.37 (3)
Nuevo Mercurio	H5	5.35	5.35±0.17 (15)
Peace River	L6	4.95	4.93 (2)
Phum Sambo	H4	5.38	5.37 (2)
Stannern	EUC	2.69	2.68±0.02 (4)
Warrenton	CO3.7	4.44	4.41 (2)
Wiluna	H5	5.29	5.27±0.07 (4)
Zagami	SNC(SHE)	2.66	2.76±0.10 (3)

Table 2.2. Average magnetic susceptibility values (Logχ in 10^{-9} m^3/kg) for meteorites with multiple specimens. Parentheses indicate the number of specimens used in the mean. * Average computed using the total summed mass of the meteorite measured along with the total summed susceptibility measured from each piece. Error listed in fourth column is ±1 standard deviation and computed for cases when there are more than two fragments of same meteorite.

Meteorite Class	Logχ 19000 Hz	A%	B%
E chondrite	5.25±0.42 (8)*	21.8±9.8 (5)*	4.8±8.67 (5)*
Fall	5.48±0.10 (4)	-	-
Find	5.01±0.51 (4)	-	-
H chondrite:	5.06±0.26 (53)*	16.0±6.3 (31)	-5.9±10.5 (31)
Fall	5.29±0.10 (22)	18.2±3.6 (12)	-10.3±9.7 (12)
Find	4.93±0.25 (31)	14.3±7.1 (19)	-3.6±10.3 (19)
L chondrite:	4.68±0.30 (50)*	13.6±6.4 (26)	-8.1±10.0 (26)
Fall	4.87±0.08 (27)	15.2±6.9 (10)	-7.5±9.2 (10)
Find	4.43±0.34 (24)	12.5±6.1 (16)	-8.6±10.8 (16)
LL chondrite	4.04±0.35 (8)	8.9±3.8 (7)	-6.9±7.2 (7)
C chondrite	4.24±0.56 (18)*	5.5±2.8 (17)*	-3.9±2.8 (17)*
Rumurutiite	2.92 (2)	3.5 (1)	-3.5 (1)
Acapulcoite	5.70 (1)	33.7 (1)	-31.5 (1)
Winonaite	4.41 (1)	-	-
Ureilite	4.59±0.38 (5)	10.1±6.6 (4)	6.4±6.7 (4)
Brachinite	3.33 (1)	10.7 (1)	-14.7 (1)
Aubrite	3.47±0.57 (7)	34.4±14.3 (5)	15.4±13.5 (5)
Howardite	3.12 (2)	5.7(2)	-0.1(2)
Eucrite: Other	2.85±0.17 (6)	5.8±3.7 (5)	-4.9±4.1 (5)
C. Donga	4.26±0.20 (12)	14.5±1.4 (12)	-18.4±3.2 (12)
Diogenite	3.43 (1)	19.9 (1)	8.0 (1)
SNC meteorite	3.01±0.22 (8)	5.8±3.5 (5)	-0.5±6.4 (5)
Lunaite	2.37 (1)	-	-

Table 2.3. Magnetic susceptibility values (Logχ in 10^{-9} m^3/kg). Parentheses indicate the number of meteorites or of meteorite fragments used in the mean. * have outliers removed. See text for outlier determination. A% and B% are defined in equations 2.4 and 2.5 respectively.

Two parameters were calculated to evaluate the anisotropy of susceptibility: 1) the degree of AMS and 2) the ellipsoid shape. These can be calculated in a variety of ways. The formulations A% for degree of AMS and B% for ellipsoid shape were chosen (Cañón-Tapia 1994; Cañón-Tapia et al. 1996). Calculations for A% and B% were as follows:

[2.4] $A\% = 100\ (1- (k_3 + k_2) / 2k_1)$,

[2.5] $B\% = 100\ (1+ (k_3 - 2k_2) / k_1)$,

where k_1 is the maximum, k_2 the intermediate and k_3 the minimum bulk volume susceptibility. A% ranges from 0 to 100 and B% ranges from -100 (oblate) to +100 (prolate). In terms of physical rock fabric, an oblate ellipsoid shape represents a dominant foliation, and a prolate ellipsoid represents a dominant lineation.

For bulk magnetic susceptibility the detection limit of the SI-2B instrument at 19000 Hz is approximately 1×10^{-6} SI, therefore for susceptibilities of about $K < 10 \times 10^{-6}$ SI there may be an increase in measurement uncertainty. These specimens are identified with an asterisk in Appendix II, and for completeness were used in calculations of class means. Additional calculations, not included in Table 2.3, show that their deletion does not significantly alter the calculated class mean although uncertainties were slightly increased. In terms of AMS, the diamagnetic sample holder displayed a minor anisotropy below the detection limit. Thus, for AMS specimens with $K < 15 \times 10^{-6}$ SI these effects resulted in lower-precision analyses. The above effects were related to sample size (i.e. very small specimens) and only affected a small number of measured specimens. The lunaite specimen and a few SNC meteorites were the only classes affected.

Specimens measured for frequency dependence were limited to minimum signal strengths of 30×10^{-6} SI. The detection limit of the Si-2B at 825 Hz is approximately 2.5×10^{-6} SI, allowing an uncertainty of about 10%.

2.1.2 *Outlier Determination*

The criterion for determining outliers is two standard deviations from the mean. Nine outliers (Happy Canyon'; NWA 801', Ingella Station; Laundry East; Lushton; Moorabie; Roosevelt County 004, 012, and 017) were identified and represent a small percentage (≤7.5% in the present study) of the total population measured. They are not used in any calculations involving meteorite classes.

All nine outliers are finds and display measured MS and/or AMS values significantly below their respective class mean (NWA 801' and Moorabie are exceptions). Weathering acts to reduce the metal content and to round metal grains thus altering the MS and AMS of a sample (Gattacceca et al. 2005). It is therefore likely that these specimens have undergone more significant degrees of weathering than other finds in their respective classes. Thus, their measured MS and AMS values are not representative of the meteorites' pristine mineralogy nor the classes. These considerations emphasise the importance of evaluating terrestrial weathering when attempting classification of meteorites using magnetic properties. Finds, falls and weathering effects are further discussed in section 2.2. In addition, distinction between falls and finds for L, H and E chondrites is maintained throughout much of this chapter.

Happy Canyon' is a possible mispairing (i.e. not related to Happy Canyon) as its MS differs significantly from another Happy Canyon specimen measured as well as the rest of the E chondrite class both in terms of MS and AMS. These relationships are further illustrated in sections 2.3.3 and 2.3.4. Happy Canyon' is therefore not used in any calculations as its possible mispairing may also reflect a possible misclassification.

NWA 801' is another possible mispairing as its AMS is significantly higher than another specimen of NWA 801 as well as the rest of the C chondrite class. Its MS falls

within two standard deviations of the mean; however, it also has the highest value measured in that class. For these reasons, NWA 801' might be a misclassification and is thus considered to be unrepresentative of the C chondrite class and was not used in any calculation of AMS or MS class averages. NWA 801' is further discussed in sections 2.3.3 and 2.3.4.

Moorabie has an MS value that is significantly higher than any other meteorite in the L chondrite class. Its MS is much more reflective of an H or E chondrite classification. This meteorite is a find with minimal crust and its relatively high MS is cause for suspicion and suggests a possible misclassification. Thus, Moorabie is not used in any calculations of L chondrite class means.

Two meteorites (Acfer 057 and Red Lake) were not fully classified in the Meteoritical Bulletin Database published by the Meteoritical Society nor in the database of the National Meteorite Collection of Canada and thus were excluded from calculations involving class means. In addition, three meteorites (Bremervorde, Cynthiana and Knyahinya) were also excluded from any class calculations because of their intermediate ordinary chondrite classifications. See section 2.3.3 for more discussion.

2.2 Factors Affecting Primary Magnetic Susceptibility

There are several effects that may alter the pristine magnetic mineralogy of meteorites and thus affect the interpretation of magnetic susceptibility measurements. The development of a fusion crust during atmospheric entry and subsequent terrestrial weathering are two of the more influential parameters affecting primary magnetic susceptibility (Rochette et al. 2001, 2003).

Because rock is a poor conductor of heat the interior of a meteorite remains relatively cool and pristine during atmospheric ablation and fusion crust formation. The chemical composition of the fusion crust remains similar to its bulk composition (Genge and Grady 1999); however, the oxidation of iron into magnetite and a corresponding decrease in metallic iron, occurring within the fusion crust during its formation, will modify the susceptibility of the sample. For meteorites with a relatively strong susceptibility (i.e. $\log\chi>4$), this effect is minor. For weakly magnetic specimens, however, the susceptibility of the crust can increase by up to 10%, affecting the overall bulk susceptibility measurement (Rochette et al. 2001). Therefore, the susceptibility of small size (i.e. low mass) specimens that have an extensive fusion crust may not be representative of the meteorites' pristine mineralogy as much of the mass will be contained in the crust. Conversely, larger specimens will contain much more pristine material relative to the fusion crust and will yield a susceptibility value more representative of their pristine mineralogy. These specimens can be readily identified in Appendices I, II and III as the extent of fusion crust and mass of the specimen are listed.

Terrestrial weathering tends to lower the susceptibility of a meteorite via the oxidation of metal. Contamination from other sources such as water and subsequent leaching can also alter the composition and chemistry of meteorites (Jarosewich 1990). Therefore, distinguishing between "finds" and "falls" for each meteorite is a fundamental step towards accurate classification. Finds are meteorites that have been found usually long after they impacted the Earth's surface and thus have been subjected to terrestrial weathering until their recovery. Falls are distinguished by a visual sighting of the meteor during its descent to Earth usually leading to a quick recovery. Due to less interaction with the terrestrial environment, falls will yield magnetic susceptibility values more representative of a meteorites' pristine mineralogy and classification than finds.

Terrestrial weathering may also influence the AMS of a meteorite by preferentially altering the corners resulting in more rounded metal grains on the exterior of the sample thus affecting the grain shape (Gattacceca et al. 2005).

Some meteorites are less resistant to terrestrial weathering and alteration than others. Aubrites, for example, due to their composition and friability, are easily altered in the Earth's environment. Therefore, the validity of scientific observations on these meteorites can decrease rapidly if they are not quickly recovered. On the other end of the spectrum, iron meteorites are the most resistant and take longer to disintegrate. They, however, can still suffer from alteration via oxidation (McSween 2000).

Brecciation can cause heterogeneity within a meteorite as the resulting clasts may be of variable size and distribution. Veining may also cause heterogeneities. Both brecciation and veining may sometimes introduce variability in susceptibility measurements among fragments of the same meteorite and also among meteorites in the same class. The effects of anisotropy and also of grain size will be discussed in later sections.

The extent of fusion crust, and find or fall status are recorded for each specimen in Appendices I, II, III. The magnetic susceptibilities and AMS of L, H and E chondrites are further subdivided into finds and falls in Table 2.3 and in Fig. 2.2 and 2.6. Brecciation, veining and other attributes present are also listed, as described by Jensen et al. (2004).

2.3 Results

In this section, experimental results for the four magnetic parameters of interest are presented. The 19000 Hz frequency data are the values used and reported in the present study unless otherwise indicated.

2.3.1 *Magnetic Susceptibility (MS)*

Mean bulk magnetic susceptibility values for each meteorite class are presented in Fig. 2.2. A clear trend can be seen in the chondrites as susceptibility increases from LL, L, H to E chondrites reflecting increasing Fe-Ni metal and Fe-Ni sulphide content. This trend is consistent with previous studies involving magnetic susceptibility (e.g. Sonett 1978; Rochette et al. 2001, 2003). Bulk susceptibility is typically consistent among specimens of different mass (i.e. size) of the same meteorite and illustrated in Fig. 2.3; a similar figure can be found in Rochette et al. 2003.

It is evident that much of the variability in magnetic susceptibility is largely due to terrestrial weathering as seen from the much lower standard deviations of falls compared to finds for L, H and E chondrites (Table 2.3). This difference is further illustrated in Fig. 2.2.

C chondrites have a large spread in susceptibility values reflecting heterogeneity within that class (Figs. 2.2 and 2.4). The subclasses C3.8-4, CM2, CR2, CO3, CV3 and CK display distinct characteristics. The CM2 subclass has distinctively lower susceptibilities than the other measured subclasses (with the exception of one CV3 specimen: NWA 2086). Similarity of the susceptibilities among the CO3 and CK and CV3 subclasses reflect the mineralogical similarities that these three subclasses share. The higher susceptibility of the CR2 reflects the known presence of abundant Fe-Ni grains within that subclass. The ability of bulk magnetic susceptibility alone to help distinguish among the various C chondrite subclasses makes it a valuable parameter for their classification, given their petrophysical complexities and fragility.

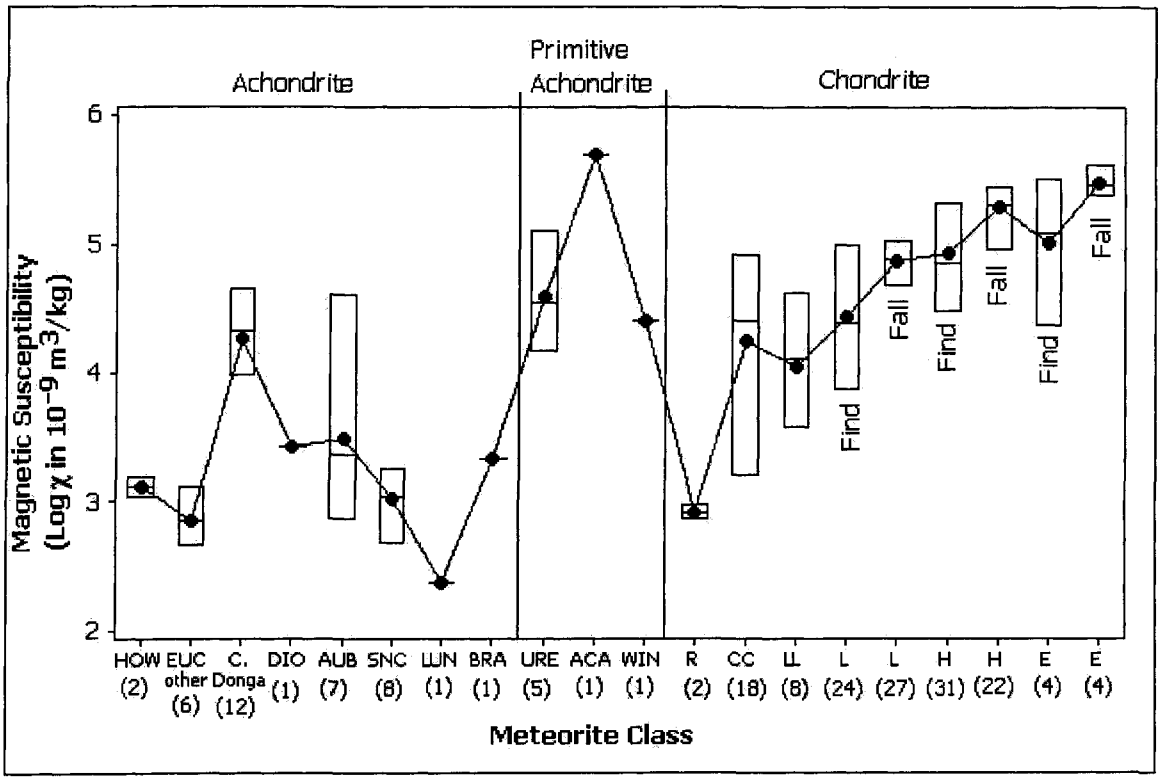

Fig. 2.2. Magnetic susceptibility (19000 Hz) versus meteorite class. Parentheses indicate the number of meteorites used in the mean, after removal of outliers. Horizontal lines indicate minimum, median and maximum values with the average represented as a dot. Abbreviations are as follows: HOW, howardite; EUC, eucrite; C. Donga, Camel Donga; DIO, diogenite; AUB, aubrite; SNC, SNC meteorite; LUN, lunaite; BRA, brachinite; URE, ureilite; ACA, acapulcoite; WIN, winonaite; R, rumurutiite; CC, C chondrite; LL, LL chondrite; L, L chondrite; H, H chondrite; E, E chondrite

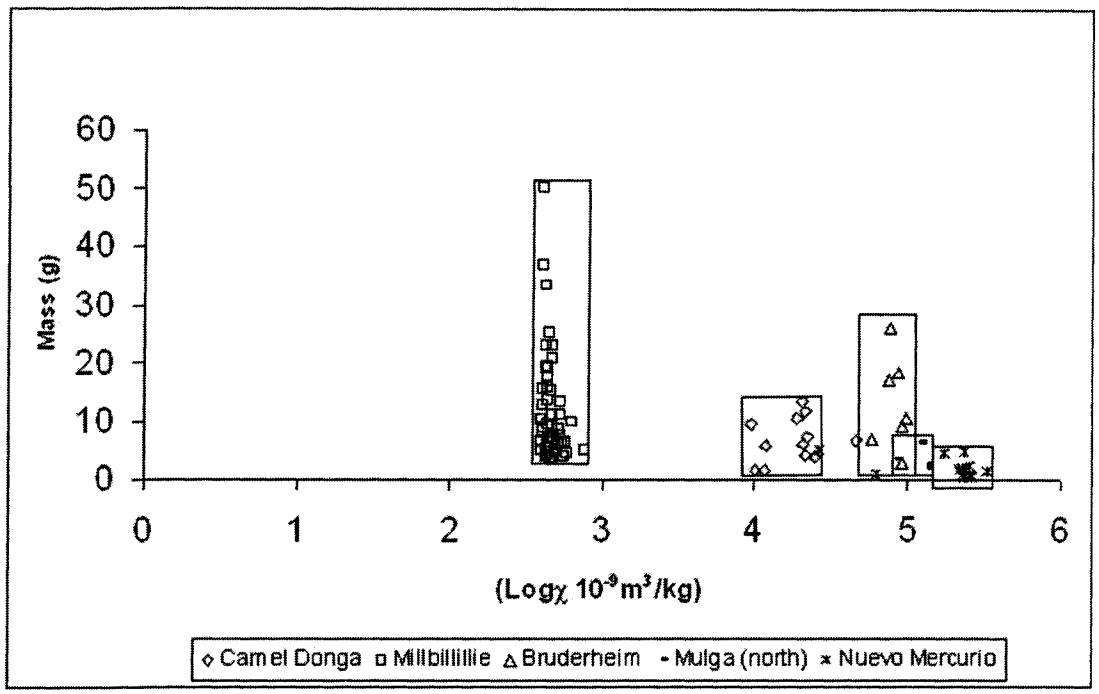

Fig. 2.3. Mass versus magnetic susceptibility (19000 Hz). The narrow spread of data for each meteorite illustrates how magnetic susceptibility of a meteorite is consistent among fragments of different mass (i.e. size).

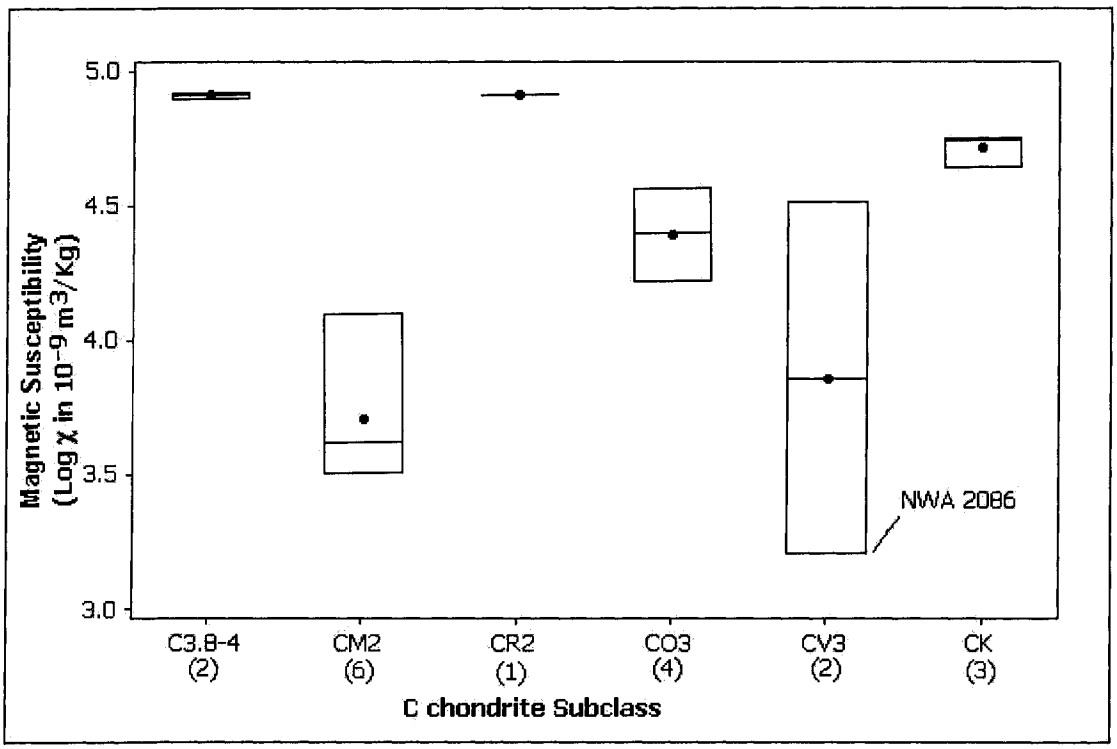

Fig. 2.4. Characterization of C chondrites using magnetic susceptibility (19000 Hz). Parentheses indicate the number of meteorites used in the mean. Horizontal lines indicate minimum, median and maximum values with the average represented as a dot. Abbreviations discussed in text.

The achondrites display more variability in susceptibility values, reflecting their complex petrogenesis. During the formation of achondrites, differentiation of the parent body caused the siderophile elements to be partitioned into a metallic core with surrounding mantle. Thus, the achondrites are depleted in the siderophile elements as a result of being the product of partial melting of the mantle material (McSween 2000). Achondrites are therefore dominated by paramagnetic minerals (e.g. Fe-Mg silicates), and are typically significantly depleted in free metal. For this reason, achondrites generally have lower magnetic susceptibility values than the undifferentiated chondrites.

The eucrites have some within-class differences that may be significant and related to provenance and history of their parent body. Camel Donga has a bulk magnetic susceptibility of 4.31, distinct from other eucrites (e.g. Millbillillie, 2.66; Stannern, 2.67). It is well documented that Camel Donga has a high metal content (~2%) likely derived from the reduction of iron in silicates under thermal metamorphism (Palme et al. 1988). This process has been noted for other eucrites but to a much smaller extent. It suggests a somewhat unique history for Camel Donga. Camel Donga is brecciated and thermally metamorphosed, perhaps from impacts and burial from ejecta and/or deep burial (Palme et al. 1988). The eucrites are thought to be basaltic crustal material and thus the differences in magnetic susceptibility may indicate heterogeneity of basaltic flows from the same parent body, or different parental bodies; although similar ^{17}O - ^{18}O fractionation trends strongly suggest a common parent body for the eucrites (McSween 2000; Drake 2001). Because of this significant difference in susceptibility, Fig. 2.2 subdivides the eucrites as 'Camel Donga' and 'other eucrites'. In addition, the eucrites are believed to share a common parent body with the diogenites and the howardites (together termed the HED meteorites). The eucrites are the basaltic flows, the diogenites are plutonic rocks and the howardites are a mixture of both eucrites and diogenites. Although only two howardites and one diogenite (two specimens) were

measured, the susceptibility of the howardites falls in-between that of the diogenites and the 'other eucrites' (Fig. 2.2). This supports the hypothesis that the howardites are a polymict breccia containing clasts of both diogenite and eucrite material.

The aubrites show a large spread in values that can be attributed to the brecciated nature of the class. Cumberland Falls has a susceptibility of 4.60, much higher than the rest of the class (Appendix II). This is likely due to the presence of high metal content chondritic clasts within that meteorite (Lorenzetti et al. 2003).

The SNC meteorites are Martian in origin and generally have a much younger crystalline age than most meteorites (McSween 1994). The spread in logχ values (Fig. 2.2, Table 2.3) may be a result of the meteorites originating from various regions in the Martian crust.

Primitive achondrites (ureilites?, acapulcoites, winonaites) display higher susceptibility values than the other achondrites. Their magnetic susceptibility is more in line with that of the chondrites (Fig. 2.2). Weathering may explain why Terra Blanca has lower MS than H chondrites, as winonaites such as Terra Blanca typically have a higher metal content. Primitive achondrites are the residues of partial melting that have undergone some metamorphism, display achondritic textures, but still retain some of their original chondritic composition (McSween 2000; Norton 2002). They are not fully differentiated like the achondrites and therefore might not be as depleted in the siderophile elements. This may explain why their susceptibilities are more chondritic than achondritic in nature.

The lone brachinite measured (Eagles Nest) yielded a susceptibility value of 3.32, much lower than the primitive achondrites but comparable to the achondrites, further supporting their reclassification as differentiated achondrites (Mittlefehldt et al. 2003). All five ureilites measured have susceptibilities above 4.15 further suggesting they are more related to the primitive achondrites than to the achondrites (Goodrich 1999).

The mesosiderite is a unique meteorite due to its unusual composition of ~50% basalt and ~50% metallic Fe-Ni. It is still unclear as to how the relatively buoyant silica rich basalt could have mixed with the much denser iron. A collision between asteroids, during which the iron core of one body mixed with the silica surface of the other, is a proposed explanation (Jensen et al. 2001). As expected on the basis of the higher metal content in the stony-iron class relative to the other measured classes, the mesosiderite has the largest susceptibility of the dataset (Appendix III).

The one lunaite and lunar soil specimen are very small in size and thus their measured values are just above the detection limit of the SI-2B instrument (Appendix II). For this reason much discretion is used in their interpretation. Dhofar 461 yielded the lowest MS value (2.37) of the entire dataset with the lunar soil giving a much higher value of 3.65; however the soil's mass is very small and only measured to the second decimal place. Because of the few magnetic measurements done on lunaites and lunar soil samples, only a preliminary discussion is included.

2.3.1.1 *Comparison with Other Databases*

Fig. 2.5, similar to Fig. 3 in Rochette et al. (2001) for database comparison, shows a comparison between the magnetic susceptibility of specimens of meteorites belonging to the National Meteorite Collection of Canada, and of specimens of the same meteorites listed in the database of Rochette et al. (2001, 2003) as well as several unpublished measurements from Rochette and co-workers (2004, pers. comm.). The database of Rochette et al. (2001, 2003) is based on a frequency of 920 Hz using the Kappabridge KLY-2 instrument. The results of the present study for a frequency of 825 Hz (on the

Sapphire SI-2B instrument) are used in the comparison to introduce as few frequency dependence effects as possible.

A calibration between instruments is provided by a comparison with a Kappabridge KLY-2 instrument at the University of Ottawa. A 19 g sample standard of MnO_2 is used. Measurements are found to be consistently lower on the Sapphire instrument, by 5% or less, in comparison to the Kappabridge. In addition, Benn and Ernst (2005) found a difference between instruments of less than 3% while measuring Cambodian soil fractions. The observed minor difference may be related to field dependence (Worm 1991; Jackson et al. 1998) as the Kappabridge uses an applied magnetic field strength of 300 A/m and the SI-2B 24 A/m. In addition, differences could also be attributed to veining or mineralogical heterogeneities among specimens of the same meteorite. However, Fig. 2.5 suggests that the difference between instruments is not appreciable when expressed using a log scale. Overall there is a strong consistency between our database and that of Rochette et al. (2001, 2003). Consistency is important as the integration of all databases is required to create a global reference for rapid classification.

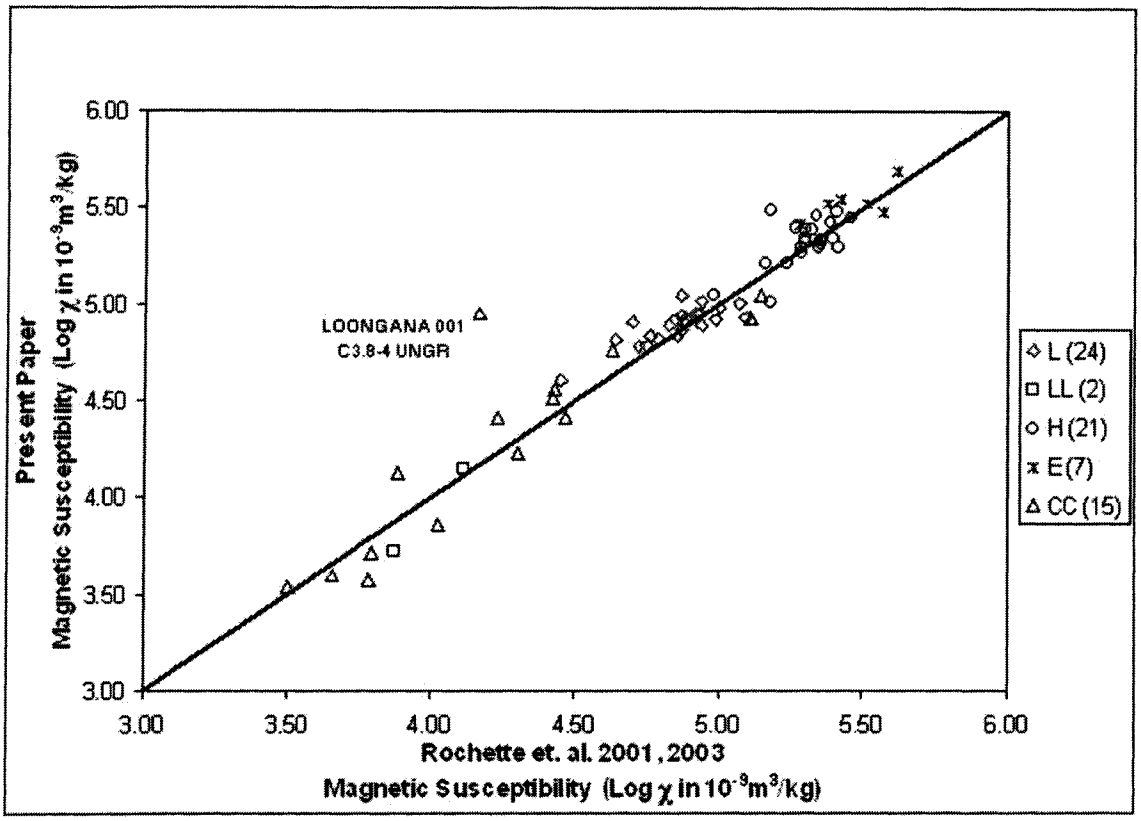

Fig. 2.5. Comparison between the magnetic susceptibility (825 Hz) of specimens of meteorites belonging to the National Meteorite Collection of Canada, and of specimens of the same meteorites listed in the database of Rochette et al. (2001, 2003). Included are several unpublished values from Rochette and co-workers.

2.3.2 *Frequency Dependence of Magnetic Susceptibility*

The study of the frequency dependence of magnetic susceptibility is important for two reasons. First, if a significant dependence is observed then a correction factor must be applied to the susceptibility measurements based on the frequency used. Second, if variability is displayed among classes then the frequency dependence of magnetic susceptibility provides another useful parameter of classification.

Frequency dependence of magnetic susceptibility is investigated by taking measurements at 825 and 19000 Hz. A detailed description of the method used can be found in section 2.1. A common standard of 19 g MnO_2 is used for both frequencies as it displays no frequency dependence. The frequency dependence of individual specimens ranges from 1 to 25.6%. The vast majority of specimens, however, have a dependence of less than 15% (Fig. 2.6). The acapulcoite, H chondrites and the diogenite display the three highest dependences while the winonaite, howardites and eucrites display the three lowest. Generally, the achondrites display more variability than the chondrites, although the H chondrites display the largest spread.

The causes of the frequency dependence of magnetic susceptibility have not been studied in great detail, even in terrestrial rocks. Theoretical arguments suggest that frequency dependence has an upper limit of ~15% (Dearing et al. 1996; Worm 1998). Much higher values, however, have been determined in some specimens (Eyre 1997).

Field dependence of magnetic minerals can be mistaken as a frequency dependence of magnetic susceptibility (Worm 1991; de Wall 2000; Jackson et al. 1998), however this cannot explain the dependence observed in the present study as both the 19000 and 825 Hz coils operate at the same applied magnetic field strength of 24 A/m.

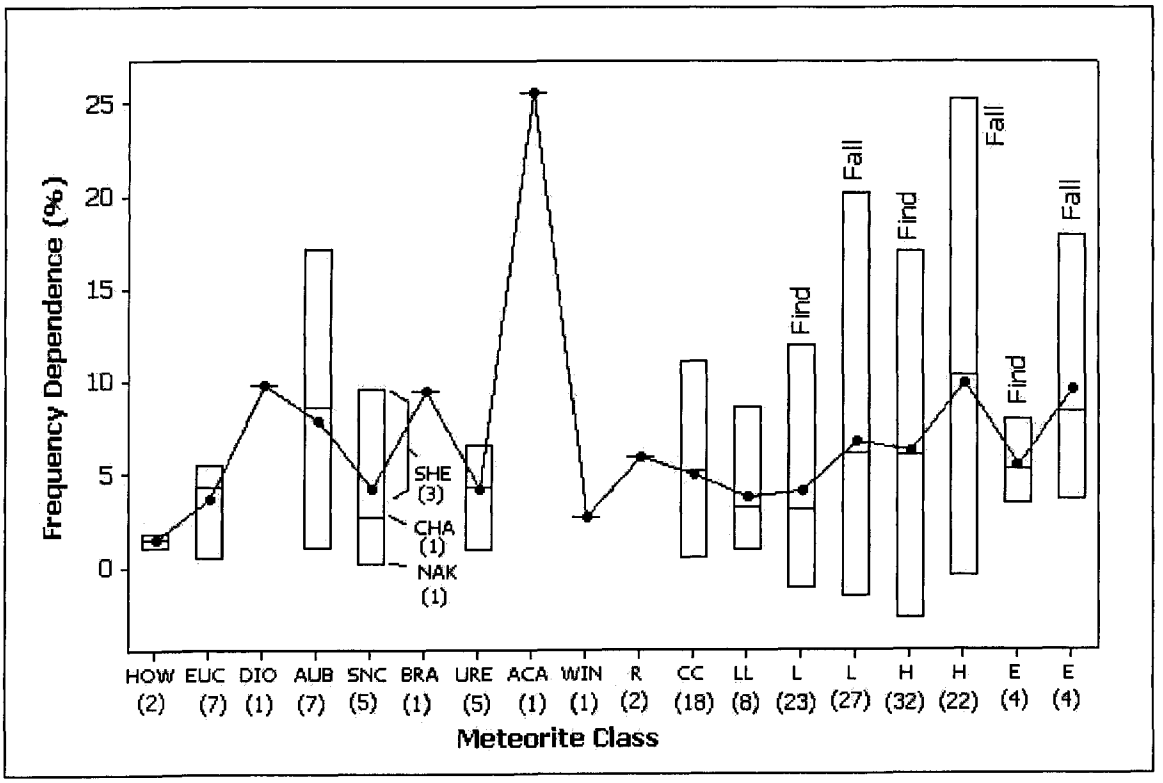

Fig. 2.6. Frequency dependence of magnetic susceptibility (19000 Hz and 825 Hz) versus meteorite class. Parentheses indicate the number of meteorites used in the mean. Horizontal lines indicate minimum, median and maximum values with the average represented as a dot. Abbreviations same as in Fig. 2.2.

It has been shown that there exists a clear frequency dependence for some paramagnetic and diamagnetic minerals that readily conduct currents at frequencies higher than 500 Hz (Ellwood et al. 1993; Puranen et al. 1995). Kukkonen and Pesonen (1983), using a frequency of 1000 Hz, found no appreciable conductivity effect for chondrites. However, there have been no studies of the conductivity effect in meteorites at greater frequencies. Metal-rich meteorites and the high conductivity associated with them may produce eddy currents, which may cause a significant decrease in susceptibility at high frequencies. In the present study a trend of increasing MS with increasing frequency dependence is observed for H chondrites (Fig. 2.7). Thus, is it likely that high conductivity of the specimen is the cause of the dependence for some of the more metal-rich samples such as the acapulcoite and several H and E chondrites. However, it is evident that not all metal-rich samples are seriously affected by this phenomenon, and thus it is very possible that there is another mechanism controlling the dependence. This is supported by the observed high dependencies of several non-metal rich samples as well as non-negligible dependencies of the L chondrites and some achondrites.

The magnetic properties of some minerals (e.g. magnetite, maghemite and hematite) are strongly dependent on grain size (Tarling and Hrouda 1993; Dearing et al. 1996; Worm 1998). The 825 Hz frequency consistently yielded slightly higher susceptibility values than the 19000 Hz frequency as expected by theory (Dearing et al. 1996; Muxworthy 2001). This bias may be explained by the proportion of grains 20-30 nm in size that exhibit superparamagnetic behaviour at 825 Hz but only single domain behaviour at 19000 Hz. For grain sizes greater than about 30 nm, there is no frequency dependence. Thus the magnitude of the dependence may be a rough indicator of the proportion of 20-30 nm size grains within the sample when using these two frequencies

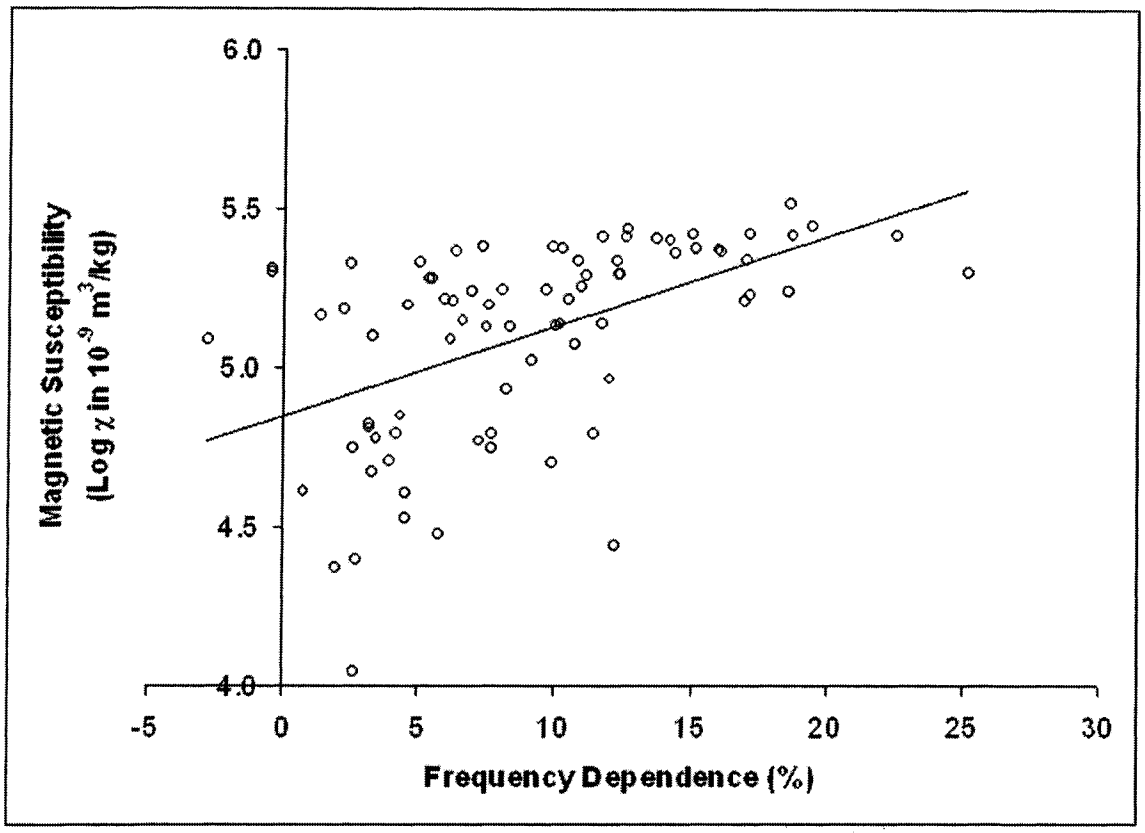

Fig. 2.7. Magnetic susceptibility of H chondrites (19000 Hz) versus frequency dependence. Linear regression trend indicated by solid line.

(Dearing et al. 1996). This behaviour has only been observed for magnetite and maghemite and has not been investigated in meteorites for other magnetic minerals. (i.e. kamacite and taenite). Considering that magnetite is the main magnetic constituent for some meteorites (e.g. C chondrites), this grain size effect may explain variations in frequency dependence among certain classes and suggest non-negligible amounts of 20-30 nm magnetite grains.

A plot of magnetic susceptibility versus frequency dependence reveals an interesting grouping in the subclasses of the C chondrites (Fig. 2.8). The CM2 specimens occupy a distinct region where MS is approximately between 3.5 and 4.2 ($\log\chi$ in 10^{-6} m^3/kg) and frequency dependence between 4 and 11%. The frequency dependence of the C3.8 and CR2 subclasses is similar to that of the CM2 subclass. The C3.8 and CR2 specimens, however, are set apart by their higher susceptibilities. Along with having similar susceptibilities, the CK, CV3 and the CO3 subclasses share a similar range of frequency dependence, again reflective of the mineralogical similarities that these three subclasses share. It should be noted that the CK, CV3 and CO3 subclasses have undergone dominant thermal metamorphism whereas the CM2 and CR2 subclasses have undergone dominant aqueous alteration. This aqueous alteration may be related to magnetite formation (Choi and Wasson 2003). The main ferromagnetic constituent of non-metamorphosed (i.e. aqueous altered) C chondrites is magnetite (Nagata 1979). Therefore, the frequency dependence of aqueous altered C chondrites may be caused by variations in magnetite grain size.

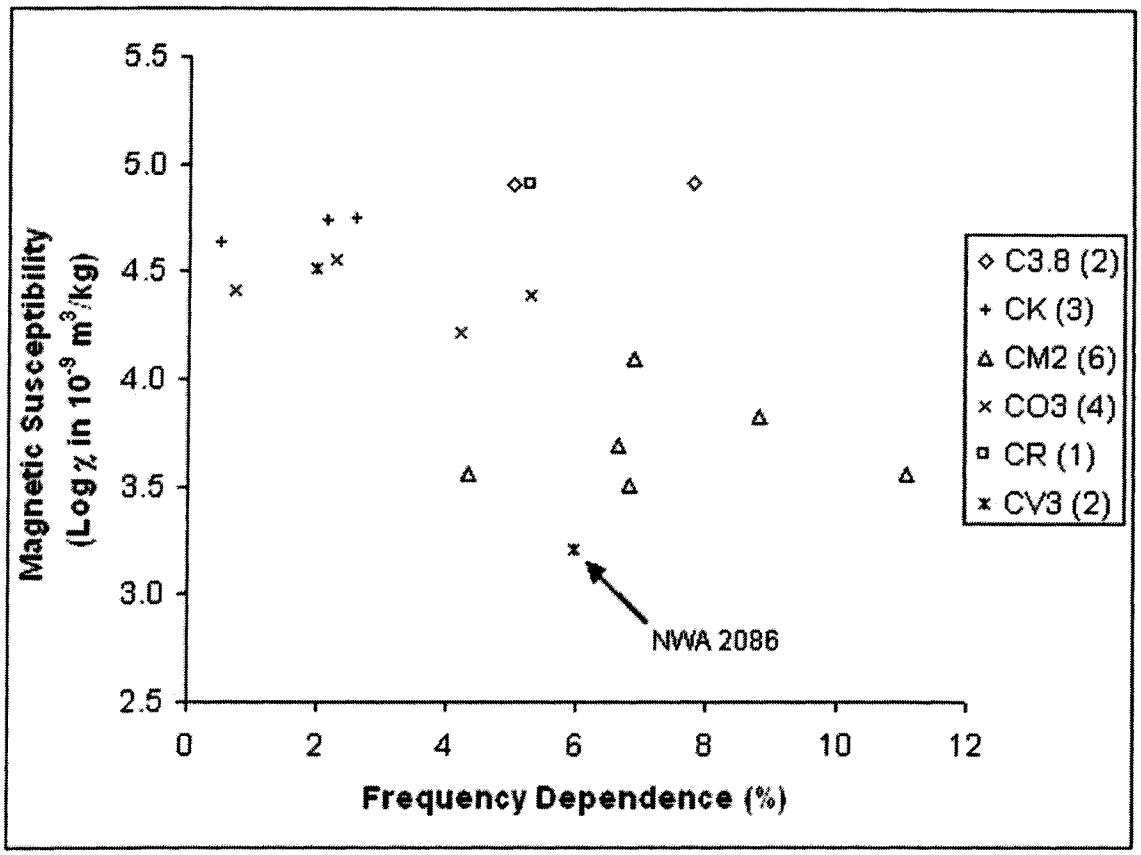

Fig. 2.8. Magnetic susceptibility (19000 Hz) versus its frequency dependence for C chondrites. The CM2 meteorites are set apart from the other subclasses. Abbreviations discussed in text.

The SNC meteorites show subclass variability with Nakhla having the lowest dependence, shergottites the highest and Chassigny falling in the middle (Fig. 2.6). Pyrrhotite is the main magnetic carrier in the shergottites (Rochette et al. 2005) and has been shown to display a magnetic susceptibility that is strongly dependent on grain size and frequency (Worm et al. 1993).

Of the four magnetic properties investigated in the present study, frequency dependence is the least understood. The observation that frequency dependence of magnetic susceptibility exists and varies among and within some meteorite classes demonstrates a potential new parameter for assisting with meteorite classification.

2.3.3 *Degree of Anisotropy of Magnetic Susceptibility (AMS)*

There are several controls on AMS that can be distinguished and are important to understand before attempting interpretations (Tarling and Hrouda 1993; Borradaile 1988). Crystalline, fabric and sample shape anisotropy are discussed below.

Crystalline anisotropy arises due to the lattice forces of the mineral creating different degrees of magnetization along each crystal axis. The magnetic susceptibility in most chondritic meteorites is dominated by ferromagnetic minerals (magnetite, titanomagetite, kamacite and taenite) which are isotropic (Rochette et al 2003). This implies that the magnetic fabric is also dominated by these same isotropic minerals. Due to this dominant isotropic contribution to the magnetic susceptibility, crystalline anisotropy is negligible for these meteorites. However, for some achondrites the magnetic mineralogy has a greater paramagnetic contribution from anisotropic silicate minerals, and thus the interpretation of AMS measurements may not be as clear in the case of achondrites. In

samples where crystalline anisotropy is non-negligible it can mask the other controls on AMS which are discussed below.

Fabric anisotropy can arise from primary emplacement (flow patterns in magma or depositional patterns in sediments). A fabric anisotropy can also arise from subsequent deformation of the material which also affects the magnetic minerals. This magnetic fabric can be related to the rock's physical fabric and thus AMS can be used as a proxy measure of fabric (Morden and Collinson 1992; Cañón-Tapia et al. 1996; Tarling and Hrouda 1993; Borradaile 1988). However, the exact relationship is not straightforward, in particular, if there is a specific and significant non-isotropic component to the magnetic susceptibility.

Another type of anisotropy arises from the sample shape, whereby the magnetic interactions of neighbouring grains take on an AMS similar to the shape of the rock itself. The majority of specimens measured are irregular in shape and some have cut surfaces. However sample shape anisotropy is believed to be negligible and minor with respect to fabric anisotropy for specimens with low bulk susceptibility i.e. $\log\chi < 5$ (Morden and Collinson 1992; Terho et al. 1993; Rochette et al. 2001, Gattacceca et al. 2005). Shape anisotropy may become a factor for some of the higher metal content specimens in the H and E chondrite classes, although such a correlation between shape and fabric axes should be rare (Rochette et al. 2001). No correction for shape has been made in this study and the AMS measurements for the acapulcoite and most H and E chondrites should be noted as having a higher degree of uncertainty due to this potential effect. However, the display of strong prolate fabric in the E chondrites with (few meteorites measured) and the weak prolate fabric displayed in H chondrites (with many meteorites measured) suggests that the results are still valid for H and E classes.

The average AMS values for each group can be found in Table 2.3. There is significant spread within a given class as well as significant differences among some

classes. H and L chondrites have AMS subdivided into finds and falls. Generally the degree of AMS of finds is lower compared to falls. This difference in AMS support the idea that weathering can alter AMS by smoothing and rounding the metal grains (Gattacceca et al. 2005).

Individual specimens showed significant degrees of AMS ranging from 1-53% (Fig. 2.9), but multiple specimens of the same meteorite typically exhibit a consistent degree of AMS. Several exceptions, however, can be identified in Appendices I and II. The aubrites, E chondrites and the acapulcoite display the highest degrees of AMS while the C chondrites display the tightest grouping. There is little difference in degree of AMS between the L and H chondrites. These AMS results match a trend previously determined by Smith, D. L. et al. (2003) based on a simpler qualitative laboratory procedure. The degree of AMS shows no correlation with petrologic type, consistent with previous studies (e.g. Martin and Mills 1980; Hamano and Yomogida 1982; Sugiura and Strangway 1983; Fujii et al. 1983; Sneyd et al. 1988; Morden and Collinson 1992).

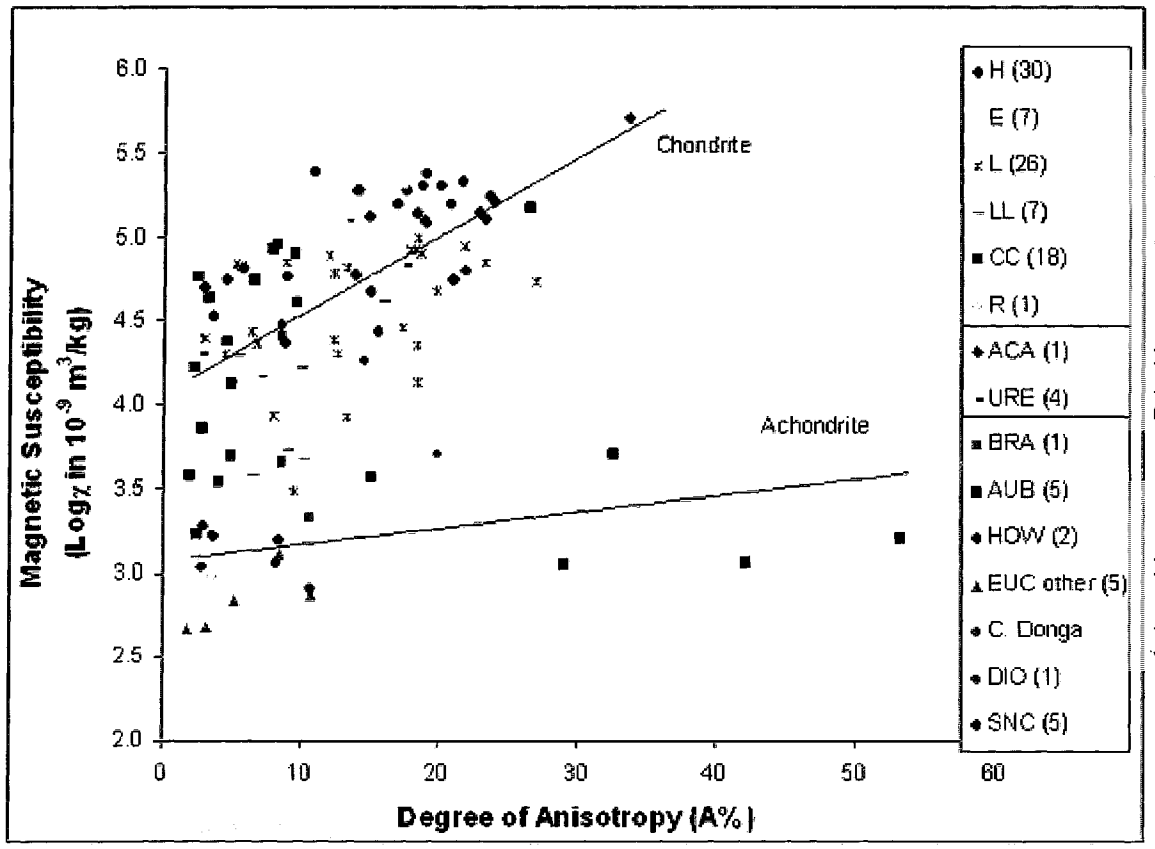

Fig. 2.9. Magnetic susceptibility (19000 Hz) versus degree of AMS. Parentheses indicate the number of meteorites plotted. Linear regression trends indicated by solid lines and computed for chondrites and achondrites (primitive achondrites not included in trend calculations). Abbreviations same as in Fig. 2.2. Colour is used to correlate legend with symbols.

Fig. 2.9 displays magnetic susceptibility versus degree of AMS. The aubrites are distinctive, being marked by their significantly higher anisotropies and corresponding lower susceptibilities. The 'other eucrites' also form an isolated region on the plot. The C chondrites are characterized by degree of AMS values with the lowest standard deviation. This tight grouping reflects the relatively primitive and unaltered nature of the C chondrites compared to the other meteorite classes. A distinct trend of increasing degree of AMS with increasing susceptibility is observed from CC to LL, L, H and E chondrites, probably largely controlled by metal content. This trend indicates a strong relationship among these meteorite classes, and perhaps a common process of origin and/or provenance. A clear distinction between chondrites and most achondrites is also observed as both groups have distinct and separate trends. The acapulcoite and ureilites are exceptions. They plot at higher susceptibilities because of their high metal content. The brachinite fits the trend of the achondrites, again suggesting a non-primitive achondritic origin.

The SNC meteorites display degrees of anisotropy ranging from 3 to 11%. Preferred orientations of pyroxenes have been noted for several basaltic shergottites and are thought to have been aligned by lava flow on the Martian surface (McSween 1994). Preferred orientation of augite grains in nakhlites have also been observed and may be related to crystallization in a subsurface sill rather than a flow. The range of values of the degree of AMS for the SNC meteorites is similar to that of the eucrites (except Camel Donga), which are thought to have formed from surface lava flows on their parent body. This suggests a common mechanism for the formation of the observed degree of AMS between the two classes.

Fig. 2.10 displays how data from different meteorite classes plot in different regions of the magnetic susceptibility versus degree of AMS plane. Each region corresponds to the mean class value ± two standard deviations. The C chondrites, E chondrites, 'other

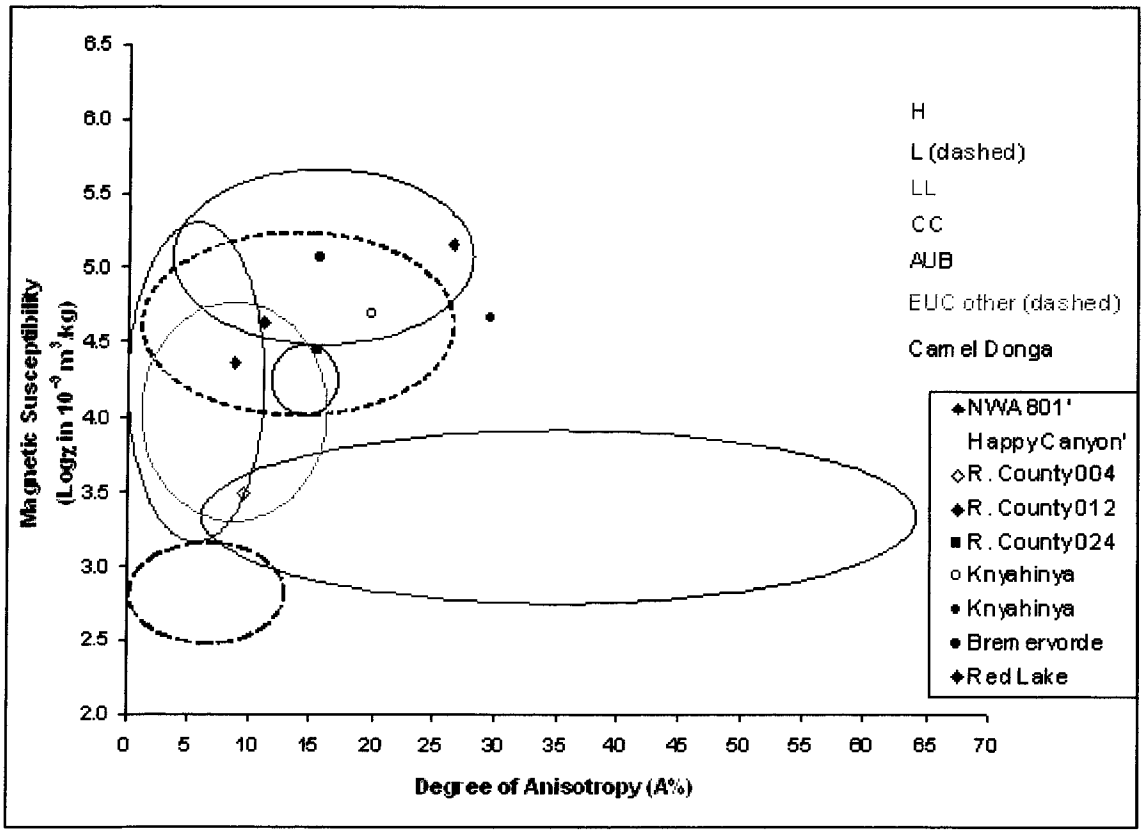

Fig. 2.10. Magnetic susceptibility (19000 Hz) versus degree of AMS. Ellipses defined using two standard deviations from the mean. Applicable outliers, unclassified and intermediate class meteorites are plotted. Apostrophes correspond to specimens with measured pairs that differ significantly in magnetic properties. No classes plotted where provenance is known. Colour is used to correlate legend with ellipses and symbols.

eucrites', Camel Donga and aubrites all occupy distinct and separate regions of the plot in relation to each other. In fact, the aubrite and eucrite regions are almost completely isolated, except for a minor overlap of LL and C chondrites with aubrites.

Outliers, unclassified and intermediate class meteorites are plotted in Fig. 2.10. NWA 801' plots far from its current C chondrite classification and closer to the H or E chondrite region. Another specimen of NWA 801 plots well within the C chondrite region suggesting that NWA 801' may be a mispairing (i.e. not related to NWA 801) or a misclassification (i.e. not a CR2). Happy Canyon' is another example of a possible mispairing or misclassification as it plots within the LL and C chondrite region, far outside the E chondrite region occupied by the other Happy Canyon specimen measured. Both Knyahinya (L/LL) specimens plot closer to a L than a LL classification. Bremervorde (H/L) plots closer to an H than an L classification. Roosevelt County 004 (L) plots well within the LL chondrite region as opposed to the L chondrite region. Roosevelt County 012 fits more with an L classification than an H, and Red Lake plots near the centre of the L chondrite region. In addition, NWA 1930 (LL) has parameters more reflective of an L classification. More data and magnetic relationships are needed to support a reclassification of the above meteorite specimens. The use of degree of AMS and magnetic susceptibility, however, appear to be a reliable discrimination tool for certain meteorite classes.

2.3.4 *Ellipsoid Shape of Anisotropy of Magnetic Susceptibility*

The ellipsoid shape parameter shows some variability among multiple specimens of the same meteorite, among meteorites in the same class, and among different meteorite classes (Fig. 2.11). The majority of specimens measured show a dominant foliation

(oblate ellipsoid), consistent with previous AMS studies (e.g. Hamano and Yomogida 1981; Sneyd et al. 1988), although they only focused on ordinary, E and C chondrites. In addition, oblate ellipsoids dominated all the chondrites measured except the E chondrites which showed no preferred fabric (about equal prolate and oblate). The C chondrites show the tightest groupings of ellipsoid shape, again reflecting their primitive nature and low degree of alteration. The aubrites, except for one specimen, show a dominant lineation fabric (prolate ellipsoid). This dominant prolate anisotropy fabric is in contrast to most other meteorite classes and may indicate a distinctive process of origin. In addition, three of the four ureilites also display prolate ellipsoids. The ellipsoid shape of AMS shows no correlation with petrologic type, consistent with previous studies (e.g. Sneyd et al. 1988).

The aubrites are thought to be related to and have a similar parent body to the E chondrites as indicated from similar ^{17}O - ^{18}O fractionation trends and mineralogy. The difference is that the aubrites were heated enough to cause nearly complete melting (Taylor el al. 1993) and differentiation, whereas the E chondrites did not differentiate. The notable presence of prolate fabric in aubrites and E chondrites may indicate common processes acting on the parent bodies and further strengthen the relationship between the aubrites and E chondrites. Most aubrites are monomict breccias composed almost entirely of enstatite. The clasts are enstatite crystals surrounded in a matrix of finer crushed enstatite. The aubrite parent body must have been impacted many times to produce such a complex internal structure. It has perhaps fragmented and then reassembled into a rubble pile body (Keil 1989; McSween 2000). The significant presence of prolate fabrics in both aubrites and E chondrites might have arisen from multiple impact events (Sugiura and Strangway 1983), with the first impact producing a foliation and a second impact, from a different direction, imparting a lineation.

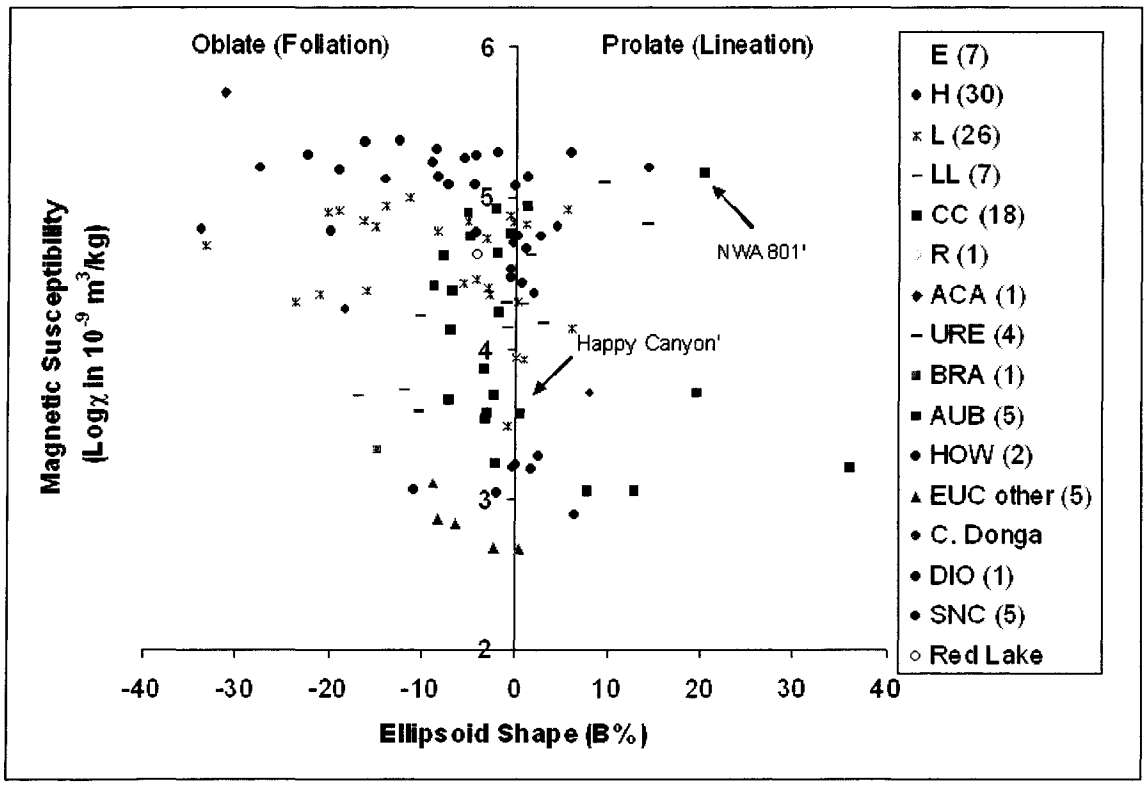

Fig. 2.11. Magnetic susceptibility (19000 Hz) versus shape of AMS. Parentheses indicate the number of meteorites plotted. Abbreviations same as in Fig. 2.2. Colour used to correlate legend with symbols.

Further evidence is displayed for the separation of Camel Donga from the 'other eucrites'. The 'other eucrites' consistently display low degrees of anisotropy (<11%) and low percentage oblate ellipsoids (<-9%) while Camel Donga displays much higher degrees of anisotropy (13-16%) and much stronger oblate fabric (-16 to -23%). Palme et al. (1988) has suggested Camel Donga's high metal content could have been derived from burial from ejecta and/or deep burial. It is thus possible that the observed AMS of oblate fabric of Camel Donga could be related to lithostatic overburden pressure causing uniaxial compression. Clearly the histories of both eucrite groups are significantly different and possibly even unrelated.

Chassigny shows the largest deviation from the SNC class in ellipsoid shape at -10.8% (oblate), all other measured SNC meteorites display prolate fabric except Shergotty which is only slightly oblate (-0.3%).

2.3.5 *Shock History and Anisotropy*

An attempt was made at correlating the degree of anisotropy with shock stage. Data on meteorite shock stage are scarce in the literature; thus the statistical viability of evaluating a possible correlation is not ideal. Sneyd et al. (1988) attempted a correlation of shock facies with amount of deformation using a simplified shock scale of increasing degree from 1 to 3 based on petrographic observations of olivine. They found a positive correlation using 15 ordinary chondrites. Stoffler et al. (1991) have since modified and determined new criteria for determining a meteorites shock stage based on alterations to olivine and plagioclase via shock metamorphism at variable pressures. These shock effects are impact-induced and thus if AMS is caused via impacts a correlation between the two should exist. However, it still remains difficult to categorize levels of shock and

as such there is an associated error of ±1 on a scale of increasing shock from S1 through S6. Recently, Gattacceca et al. (2005) observed a positive correlation between AMS and shock stage with L chondrites using the shock classification criteria of Stoffler et al. (1991), although there was much data overlap.

Shock stages used in the present study are from the literature (Stoffler et al. 1991; Scott et al. 1992; Bennet and McSween 1996; Rubin 2004; Friederich et al. 2004). Shock stages for NWA 1112, NWA 1279 and NWA 1945 are found in the database of the National Meteorite Collection of Canada. If there is a conflicting estimate of shock stage among the studies then the classification of Stoffler et al. (1991) is used.

There are only a few shock stage classifications for the ordinary chondrites evaluated in the present study and thus not enough for a statistical evaluation. However, of the seventeen C chondrites measured for AMS twelve have a pre-determined shock stage classification (Fig. 2.12). With the exception of Cold Bokkeveld, all of the C chondrites of shock stage 1 are tightly clustered. Although only two S2 and two S3 C chondrites are evaluated they have the higher degrees of AMS. Further work is needed to evaluate any possible trends such as increasing AMS with increasing shock stage.

Cold Bokkeveld is a CM2 and like most CM2 meteorites has undergone very little shock metamorphism. However, its anisotropy is relatively high and far outside the main cluster for the rest of the CM2 meteorites. Chondrule elongation has been observed in this meteorite (Scott et al. 1992) and correlates with the observed degree of AMS; however, its S1 shock classification suggests a non-shock mechanism must be responsible for its deformation. Similarly, the L chondrite Umbarger has a very low degree of AMS for its S4 shock classification.

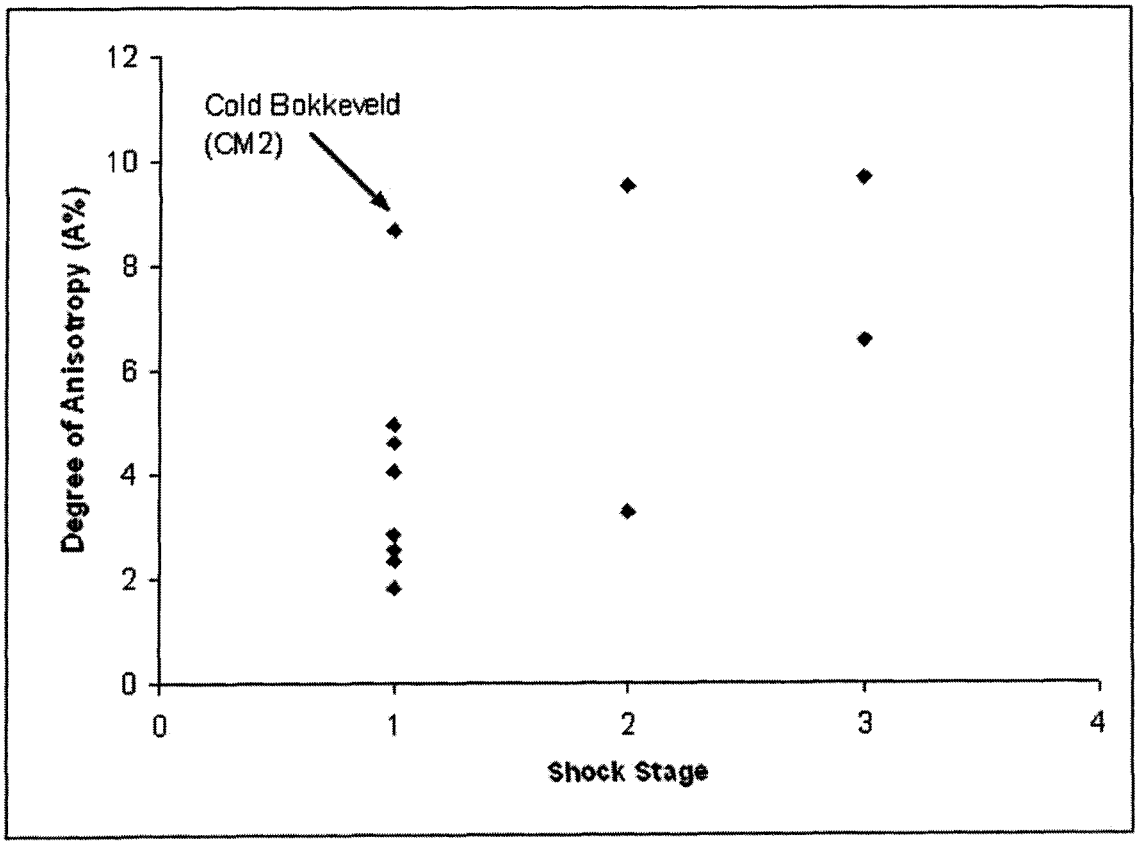

Fig. 2.12. Degree of AMS versus shock stage for C chondrites.

Due to the limited datasets of studies comparing meteorite AMS and shock stage, an error in shock stage of ±1 and much data overlap, a correlation between these two variables cannot be conclusively made. However, this information encourages the idea put forth by earlier studies (e.g. Hamano and Yomogida 1981; Sneyd et al. 1988; Morden and Collinson 1992; Scott et al. 1992) that the fabric of several classes of meteorite was produced via high velocity impacts.

2.4 Discussion

The presence of a physical fabric within a meteorite can provide insights into its origin and formation, which can be further applied to the evolution of the solar system. The measurements of magnetic properties, in particular data on the degree and ellipsoid shape of AMS (acquired as part of the present study), contribute important new information in this respect.

Three phases of parent body evolution are recognised (Hamano and Yomogida 1981 and 1982; Morden and Collinson 1992): (1) accretionary, (2) metamorphic (differentiation for achondrites) and (3) destructive (i.e. break-up of the parent body). The accretionary phase can be further subdivided into two distinct steps: (1) loose agglomeration of proto-planetary material and (2) consolidation by shock compression via impact on the surface of the parent body.

Anisotropy development was originally attributed to lithostatic pressure due to overburden material i.e. load compaction during crystallization during the accretionary phase (Stacey et al. 1961; Martin and Mills 1980). Compaction would cause flattening and reorientation of the Fe-Ni metal grains, and was used to explain the observed negative correlation between anisotropy and porosity. Dodd (1965) observed the

orientation of chondrules in chondrites to investigate the petrophysical fabric present and concluded that accretionary sedimentation of the chondrules during formation was the most probable cause of the anisotropy. A more recent hypothesis suggests that the observed anisotropy is a result of shock welding of loosely agglomerated material via a hypervelocity impactor i.e. colliding planetesimals (Hamano and Yomogida 1981 and 1982; Morden and Collinson 1992).

Sugiura and Strangway (1983) support the impact hypothesis; however, they suggest the destructive phase as the time of anisotropy formation due to the correlation between high shock intensity and high anisotropy. On the other hand, there are theoretical reasons for discounting the destructive phase. Meteorite impacts would give high strain rates resulting in fracturing and thus little penetrative deformation (Hamano and Yomogida 1982; Morden and Collinson 1992). This line of argument would seem to discount the development of anisotropy in the later phases of parent body history except for weakly anisotropic meteorites (Hamano and Yomogida 1981).

Further evidence suggesting that impacts produced the anisotropy is seen by a correlation between meteorite shock facies and degree of AMS. The higher the shock level the larger the observed anisotropy. This trend was observed in ordinary chondrites (Sneyd et al. 1988; Gattacceca et al. 2005) and the current study encourages application of this idea to C chondrites. This is strong evidence that impacts are the primary mechanism of fabric formation for several classes of chondrite.

Although chondrites and achondrites have the same fabric, the evolution of the achondrite parent bodies differs significantly from that of the chondrites as differentiation has occurred. For this reason, the observed anisotropy of achondrites in the present study cannot be primary and therefore must be secondary occurring near the end of differentiation or during the destructive phase so as to be preserved. Since fabric formation must be a late process in achondritic parent bodies, the similar fabric observed

in chondrites suggests this could have been the dominant phase. This strengthens the hypothesis that fabric formation occurred in the later phases of stony meteorite parent body evolution.

It is still possible that chondrites experienced fabric-inducing shock during metamorphism. The degree of metamorphism in chondritic material is less than that in achondritic material and does not completely destroy the internal fabric. As mentioned earlier, there is a lack of correlation between anisotropy and petrologic type suggesting that metamorphism is not a cause of the deformation. However, the timing may correlate with the superimposed effect of impact occurring during a time of regional metamorphism. During such a time the rock temperature will be elevated and thus be more susceptible to fabric production by an impact.

Previously in the literature, AMS has only been studied on ordinary, E, and C chondrites and a few achondrites with oblate fabrics observed in most cases. (e.g. Martin and Mills 1980; Hamano and Yomogida 1982; Sugiura and Strangway 1983; Sneyd et al. 1988; Morden and Collinson 1992). Furthermore, Gattacceca et al. (2005) is the only study with a substantial AMS database using L chondrites. Our results support and expand on these previous studies both in terms of magnetic susceptibility and AMS. The present study substantially increases the number of classes studied with the addition of multiple achondrite classes as well as significantly increasing the number of specimens measured per class, giving a better overall picture of the various relationships and trends among the meteorite classes. In addition, individual meteorite specimens have had multiple parameters determined for each, which is ideal for characterization and has not generally been done in past studies.

Dominant prolate fabrics have not typically been observed in previous AMS studies on meteorites due to the small number of available meteorites and classes measured. The discovery in the present study of both strong lineations and foliations among and

within meteorite classes of chondritic and achondritic material suggests common mechanisms of formation. Positive correlations between the degree of AMS and shock stage have now been observed for several classes of chondrite. This is mounting evidence that impacts are the primary mechanism of fabric formation for several classes of chondrites and possibly achondrites. It is, however, also likely that not all meteorite classes nor all meteorites in a class have achieved their fabric from impacts. The composition and low AMS of eucrites and the SNC meteorites suggest possible magmatic processes for generation of their fabrics. Camel Donga's fabric may be related to overburden pressure of a regional extent. Moreover, Cold Bokkeveld with a high degree of AMS and low shock stage, and Umbarger with a low degree of AMS and high shock stage attest to a non-impact origin for fabric formation. This suggests a complex multi-mechanism origin for anisotropy formation for stony meteorites (more so than previously thought), likely dominated by impacts, but not exclusively in all classes; and occurring in the later phases of parent body evolution.

Conclusions

This thesis has investigated two non-destructive techniques of meteorite characterization: bulk density determination using 3D laser imaging, and magnetic susceptibility. These properties are powerful tools for the characterization of meteoritic material and, subsequently, for the characterization of the solar system from which the material has been derived.

In Chapter I (Part I), eleven meteorite fragments which vary in shape, size, surface roughness, porosity and reflectance have been imaged and had their densities determined using 3D laser imaging. An auto-synchronized laser camera raster scanned the surface features of each meteorite without contact and to a high degree of precision. Visualization software was used to align several scans into a closed model and to compute its volume. The mass being pre-determined, the density was easily computed as the ratio of mass over volume. The technique took 90 minutes or less to complete per meteorite, including image data acquisition and model building.

The densities determined using 3D laser imaging compare very well with previously published values (Britt and Consolmagno 2003) with an average difference of 3.4%. The precision of the technique is better than 1%. Meteorite size did not appear to pose a problem during the imaging process nor bias density calculations. Due to the limitations of conventional techniques, the volumes determined using 3D laser imaging could be a more accurate estimate of the meteorites' bulk volume.

This study demonstrated that 3D laser imaging is a very effective tool for determining the bulk density of soluble, fragile and/or porous material without causing harmful alteration or contamination. It is the least invasive method of density measurement currently in use.

In an effort to extract more information from the 3D laser image data, a semi-quantitative pilot approach of meteorite surface roughness description has been developed using the aforementioned eleven meteorite fragments (Chapter I, Part II). The surface roughness has been evaluated by varying the surface tolerance during the polygonalization process and relating this change to the percentage of file compression. Norton County and Millbillillie display the highest surface roughness while the larger Pultusk (276g) and Mocs (151g) fragments display the lowest. These results are in agreement with naked-eye visual inspection. The extent at which the meteorite surface is covered by a fusion crust appears to be the biggest factor influencing the overall surface roughness.

This pilot study has demonstrated the potential for 3D image data acquired with the LCS to lead surface roughness information. It will have to be refined considerably before a reliable quantitative relationship between the number of triangles used to map the topology of 3D models and surface roughness is established.

In addition to volume measurements, 3D images of rock samples can yield detailed information on surface properties and texture from a distance (Samson et al. 2004). In the context of planetary exploration, 3D laser imaging could readily be used for semi-autonomous geological investigations. A laser scanner could be mounted on a roving robot exploring its environment (Herd et al. 2003; Smith et al. 2005b; Piechocinski and Sasiadek 2005). Up close a robotic arm could sample a piece of rock and precisely rotate it relative to the camera for volumetric imaging allowing for density calculations. From a distance of one metre, a highly-precise laser scanner like the LCS can accurately image individual rock samples. Diagnostic features, like bedding planes and vesicles, can be identified. Furthermore, there is also potential for grain size, shape and arrangement to be resolved, and reflection intensity yielding information on mineral constituents. From a distance of several metres, the LCS has the capability to map the

surroundings in three dimensions. This information could be used to plot the course of the robot as it moves around its environment selecting only the most interesting geomaterials for close up tests. This would allow for an efficient use of exploration time and resources.

Neptec Design Group has designed the LCS for the rigors of the space environment. The instrument has been demonstrated during Missions STS-105 (August 2001) (Samson et al. 2001, 2004) and STS-114 (July 2005) of Orbiter Discovery to the International Space Station. Once optimized for weight and size, the LCS could be a very serious candidate for robotic planetary exploration.

In Chapter II, classification of meteorites using magnetic properties was investigated with the objective of non-destructively and accurately defining a range of parameters for each stony meteorite class. Four parameters of magnetic susceptibility [bulk (mean) value, frequency dependence, degree of anisotropy and ellipsoid shape] have been tested as a discriminant tool using 321 stony meteorites from the National Meteorite Collection of Canada. Combined, these parameters provide robust discrimination among different meteorite classes.

Magnetic susceptibility provides a reliable base for classification as it is governed by metal content, increasing from LL, L, H to E chondrites within the 3.6 to 5.6 $\log\chi$ (in 10^{-9} m^3/kg) range. Achondrites display more variability in susceptibility values which reflect their more complex petrogenesis with differentiated achondrites ranging in $\log\chi$ from 2.4 to 4.7 and primitive achondrites from 4.2 to 5.7.

A plot of magnetic susceptibility versus degree of AMS provides the best discrimination among meteorite classes as the C chondrites, E chondrites, 'other eucrites', Camel Donga and aubrites all occupy distinct and separate regions in relation to each other. In addition, the aubrites and 'other eucrites' occupy nearly completely isolated regions from all measured classes on the plot.

Degrees of AMS range from 1 to 53% with both oblate and prolate ellipsoids dominantly present and with variations among meteorite classes. Frequency dependence is observed, using 19000 Hz and 825 Hz, with variations in magnitude among meteorite classes and individual specimen dependence ranging from 1.0 -25.6%. Frequency dependence among meteorite classes had not been studied in the past and the presence of certain class variations demonstrates its potential as a new tool for meteorite discrimination. In addition, comparison of published data acquired at different frequencies may be better interpreted if frequency dependence is taken into account.

The aubrite class is the most distinct and is marked by high degrees of anisotropy, low bulk magnetic susceptibility and prolate fabric. The E chondrites show no preferred fabric (about equal prolate and oblate) and the C chondrites display subclass distinctions in magnetic susceptibility and frequency dependence. In addition, the ureilites display a significant prolate fabric. The eucrite Camel Donga is set apart from other eucrites, being marked by higher bulk magnetic susceptibility, degree of anisotropy and degree of oblate ellipsoid shape. The SNC meteorites show subclass distinction in frequency dependence and Chassigny is set apart with a relatively strong oblate fabric.

Many different meteorite classes have been identified and multiple parent bodies are known to have existed, seen from distinct ^{17}O - ^{18}O fractionation trends and chemical compositions. Therefore, it is likely that there are several different origins for the formation of meteorite fabric. This is supported by the presence of both lineations and foliations of differing magnitudes. Anisotropy can be imparted more than once, altering a previously formed fabric. Hypervelocity impacts were likely the primary mechanism occurring in the later phases of parent body evolution for most stony meteorite classes.

References

Bates R. L. and Jackson J. A. 1987. *Glossary of Geology, 3rd Ed.* Alexandria, Virginia: American Geological Institute. 788 p.

Benn K. and Ernst, R. 2005. Measurement of the magnetic susceptibility of Cambodian soils as an aid in the improvement of landmine detection capabilities. In: Katsube, T.J. and Das Y. (Eds.). Electromagnetic Characteristics of Cambodian Soil: Implication for Landmine Detection in Soil Containing Ferromagnetic Minerals. *Geological Survey of Canada Bulletin.* In Press.

Bennett M. E. and McSween Jr. H. Y. 1996. Shock features in iron-nickel metal and troilite of L-group ordinary condrites. *Meteoritics and Planetary Science* 31:255-264.

Beraldin J-A., El-Hakim S. F. and Cournoyer L. 1993. Practical range camera calibration. *Proceedings of SPIE* 2067:21-30.

Borradaile J. G. 1988. Magnetic Susceptibility, petrofabrics and strain. *Tectonophysics* 156: 1-20.

Britt D. T. and Consolmagno G. J. 2003. Stony meteorite porosities and densities: A review of the data through 2001. *Meteoritics and Planetary Science* 38(8):1161-1180.

Cañón -Tapia, E. 1994. AMS parameters: Guidelines for their rational selection. *Pure and Applied Geophysics* 142:365-382.

Cañón -Tapia E., Walker G.P.L and Herrero-Bervera E. 1996. The internal structure of lava flows – insights from AMS measurements I: Near-vent a'a. *Journal of Volcanology and Geothermal Research* 70:21-36.

Cassidy W. A. 2003. *Meteorites, ice and Antarctica: A personal account.* Cambridge University Press. 349 p.

Choi B-G and Wasson J. T. 2003. Microscale oxygen isotopic exchange and magnetite formation in the Ningqiang anomalous carbonaceous chondrite. *Geochimica et Cosmochimica Acta* 67(23):4655-4660.

Consolmagno G. J. and Britt D. T. 1998. The density and porosity of meteorites from the Vatican Collection. *Meteoritics and Planetary Science* 33(6):1231-1240.

Dearing J. A., Dann R. J. L., Hay K., Lees J. A., Loveland P. J., Maher B. A. and O'Grady K. 1996. Frequency-dependent susceptibility measurements of environmental materials. *Geophysical Journal International* 124:228-240.

Dodd R. T. 1965. Preferred orientations of chondrules in chondrites. *Icarus* 4:308-316.

Drake M. J. 2001. The eucrite/Vesta story. *Meteoritics and Planetary Science* 36:501-513.

Dunlop D. J. and Ozdemir O. 1997. *Rock magnetism: fundamentals and frontiers.* Cambridge University Press. 573 p.

Ellwood B. B., Terrell G. E. and Cook W. J. 1993. Frequency dependence and the electromagnetic susceptibility tensor in magnetic fabric studies. *Physics of the Earth and Planetary Interiors* 80:65-74.

Eyre J. K. 1997 Frequency dependence of magnetic susceptibility for populations of single domain grains. *Geophysical Journal International* 129:209-211.

Friedrich J. M., Bridges J. C., Wang M-S. and Lipschultz M. E. 2004. Chemical studies of L chondrites. VI: Variations with petrologic type and shock-loading among equilibrated falls. *Geochimica et Cosmochimica Acta* 68(13):2889-2904.

Fujii H., Keisuke I., Miyamoto M. and Hamano Y. 1983. Shape of Fe-Ni grains and magnetic susceptibility anisotropy in Antarctic chondrites. *Memoirs of National Institute of Polar Research,* Special Issue 30:389-401.

Gattacceca J., Rochette P., Denise M., Consolmagno G. and Folco L. 2005. An impact origin for the foliation of chondrites. *Earth and Planetary Science Letters.* In Press.

Genge M. J. and Grady M. M. 1999. The fusion crusts of stony meteorites: Implications for the atmospheric reprocessing of extraterrestrial materials. *Meteoritics and Planetary Science* 34:341-356.

Goodrich C. A. 1999. Are ureilites residues from partial melting of chondritic material? The answer from MAGPOX. *Meteoritics and Planetary Science* 34:109-119.

Hamano Y. and Yomogida K. 1981. Magnetic susceptibility anisotropy of chondritic meteorites. *Rock Magnetism and Paleogeophysics* 8:75-80.

Hamano Y. and Yomogida K. 1982. Magnetic anisotropy and porosity of Antarctic chondrites. *Memoirs of National Institute of Polar Research,* Special Issue 25:281-290.

Herd R., Spray J., Samson C., Miller S. and Christie I. 2003. 3D imaging and modeling with a space-qualified laser camera system: Development of terrestrial applications and potential for planetary exploration. 34th *Lunar and Planetary Science Conference* (Abstract #1718). Houston, USA.

Hirt A. M. 2004, Institute of Geophysics, 8093 Zurich, Switzerland, pers. comm.

Jarosewich E. 1990. Chemical analysis of meteorites: A compilation of stony and iron meteorite analysis. *Meteoritics* 25:323-337.

Jackson M., Moskowitz B., Rosenbaum J., Kissel C. 1998. Field-dependence of AC susceptibility in titanomagnetites. *Earth and Planetary Science Letters* 157:129-139.

Jensen M. R., Jensen W. B., Black A. M. and Carion A. 2001. *Meteorites from A to Z.* USA: Published by Jenson M. R. 224 p.

Jensen M. R., Jensen W. B., Black A. M. and Carion A. 2004. *Meteorites from A to Z,* 2nd Ed. USA: Published by Jenson M. R. 275 p.

Keil K. 1962. Quantitav-erzmikroskopische integrationsanalyse der chondrite. *Chemie der Erde 22*:281-348.

Keil K. 1989. Enstatite meteorites and their parent bodies. *Meteoritics* 24:195-208.

Kukkonen I. T. and Pesonen L. J. 1983. Classification of meteorites by petrophysical methods. *Bulletin of the Geological Society of Finland* 55(2):157-177.

Lewis J. S. 1996. *Mining the sky: Untold riches from the asteroids, comets and planets.* USA: Addison-Wesley. 274 p.

Lorenzetti S., Eugster O., Busemann O., Marti K., Burbine H., and McCoy T. 2003. History and origin of aubrites. *Geochimica et Cosmochimica Acta* 67(3):557-571.

Martin P. M. and Mills A. A. 1980. Preferred chondrule orientations in meteorites. *Earth and Planetary Science Letters* 51:18-25.

McSween H. 1994. What we have learned about Mars from the SNC meteorites. *Meteoritics* 29:757-779.

McSween H. 2000. *Meteorites and their parent planets,* 2nd Ed. Cambridge University Press. 310 p.

Mittlefehldt D. W., Bogard D. D., Berkley J. L. and Garrison D. H. 2003. Brachinites: Igneous rocks from a differentiated asteroid. *Meteoritics and Planetary Science* 38(11):1601-1625.

Morden S. J. and Collinson D. W. 1992. The implications of the magnetism of ordinary chondrite meteorites. *Earth and Planetary Science Letters* 109:185-204.

Muxworthy A. R. 2001. Effect of grain interactions on the frequency dependence of magnetic susceptibility. *Geophysical Journal International* 144:441-447.

Nagata T. 1979. Meteorite magnetism and the early solar system magnetic field. *Physics of the Earth and Planetary Interiors* 20:324-341.

Norton R. O. 2002. *The Cambridge encyclopedia of meteorites.* Cambridge University Press. 354 p.

Palme H., Wlotzka F., Spettel B., Dreibus G. and Weber H. 1988. Camel Donga: A eucrite with a high metal content. *Meteoritics* 23:49-57.

Piechocinski S. P. and Sasiadek J. Z. 2005. Experimental determination of relative motion measurement accuracy for an auto-synchronous triangulation scanning laser camera. *Proceedings of SPIE* 5791:208-217.

Puranen R., Poikonen A. and Puranen M. 1995. Frequency dependence and the electromagnetic susceptibility tensor in magnetic fabric studies – a discussion. *Physics of the Earth and Planetary Interiors* 89:145-147.

Rioux M. 1984. Laser Range Finder based on synchronized scanners. *Applied Optics* 23(21):3837-3844.

Rochette P., Sagnotti L., Consolmagno G., Folco L., Maras A., Panzarino F., Pesonen L., Serra R. and Terho M. 2001. A magnetic susceptibility database for stony meteorites. *Quaderni di Geofisica* 18:1-30.

Rochette P., Sagnotti L., Bourot-Denise M., Consolmagno G., Folco L., Osete M. L. and Personen L. 2003. Magnetic classification of stony meteorites: 1. ordinary chondrites. *Meteoritics and Planetary Science* 38(2):251-268.

Rochette P., Gattacceca J. and Chevrier V. 2005. Matching Martian crustal magnetization and meteorite magnetic properties. *Meteoritics and Planetary Science* 40(4):529-540.

Rubin A. E. 2004. Postshock annealing and postannealing shock in equilibriated ordinary chondrites: Implications for the thermal and shock histories of chondritic asteroids. *Geochimica et Cosmochimica Acta* 68(3):673-689.

Samson C., English C., Deslauriers A., Christie I., and Blais F. 2001. Imaging and tracking elements of the International Space Station using a 3D autosynchronized laser scanner. *Acquisition, tracking, and pointing XVI, Proceedings of SPIE* 4714:87-96.

Samson C., English C., Deslauriers A., Christie I., Blais F., and Ferrie F. 2004. Neptec 3D Laser Camera System: From space mission STS-105 to terrestrial applications. *Canadian Aeronautics and Space Journal* 50(2):115-123.

Scott E. R, Keil K. and Stoffler D. 1992. Shock metamorphism of carbonaceous chondrites. *Geochimica et Cosmochimica Acta* 56:4281-4293.

Smith D. L. 2003. Magnetic susceptibility of stony meteorites from the National Meteorite Collection of Canada. B.Sc. Thesis. Dept. of Earth Sciences, Carleton University.

Smith D. L., Ernst R. E., and Herd, R. 2003. Magnetic susceptibility of stony meteorites from the National Meteorite Collection of Canada. 34th *Lunar and Planetary Science Conference* (Abstract #1939). Houston, USA.

Smith D. L., Ernst R. E., Herd R. K. and Samson, C. 2004. Petrophysical characterization of stony meteorites using low field magnetic susceptibility: Initial results from anisotropy measurements (Abstract #1243). *AGU/CGU/SEG/EEGS Joint Assembly.* Montreal, Canada.

Smith D. L., Ernst R. E., Samson C. and Herd R. 2005a. Stony meteorite characterization by non-destructive measurement of magnetic properties. *Meteoritics and Planetary Science.* In Press.

Smith D. L., Samson C., Herd R., Christie I., Sink J-E, Deslauriers A. and Ernst R. E. 2005b. Bulk density determination of meteorites using 3D laser imaging: A new tool for geomaterial characterization and space exploration. *Fifth Canadian Space Exploration Workshop* (Abstract #46). Montreal, Canada.

Smith D. L., Samson C., Herd R., Christie I., Sink J-E, Deslauriers A. and Ernst R. E. 2005c. Measuring the bulk density of meteorites and rock samples non-destructively using 3D laser imaging. *36th Lunar and Planetary Science Conference* (Abstract #1372). Houston, USA.

Smith D. L., Samson C., Herd R., Deslauriers A., Sink J-E, Christie I. and Ernst R. E. 2005d. Non-destructive Measurement of Meteorite Bulk Density Using 3D Laser Imaging. *Journal of Geophysical Research: Planets*. Accepted.

Smith I. C., Hudson R. and Cournoyer L. 2003. Design of laser optics used in Neptec 3D Laser Camera System for low earth orbit environment. *Proceedings of the Fourth Canadian-International Composites Conference*. Ottawa, Canada.

Sneyd D. S., McSween H. Y., Sugiura N., Strangway D. W., and Nord Jr. G. L. 1988. Origin of petrofabric and magnetic anisotropy in ordinary chondrites. *Meteoritics* 23:139-149.

Sonett C. P. 1978. Evidence for a primordial magnetic field during the meteorite parent body era. *Geophysical Research Letters* 5(2):151-154.

Stacey F. D., Lovering J. F. and Parry L. G. 1961. Thermomagnetic properties, natural magnetic moments and magnetic anisotropies of some chondritic meteorites. *Journal of Geophysical Research* 66(5):1523–1533.

Stoffler D., Keil K. and Scott R. D. 1991. Shock metamorphism of ordinary chondrites. *Geochimica et Cosmochimica Acta* 55:3845-3867.

Stupavsky M. 2005, 1420 Simmers Ave., N9Y 2T2, Kingsville, ON, Tel: 519-733-6156 Fax: 519-733-3340 pers. comm.

Sugiura N. 1977. Magnetic properties and remanent magnetization of stony meteorites. *Journal of Geomagnetism and Geoelectricity* 29:519-539.

Sugiura N. and Strangway D. W. 1983. Magnetic anisotropy and porosity of chondrites. *Geophysical Research Letters* 10(1):83-86.

Tarling D. H. and Hrouda F. 1993. *The magnetic anisotropy of rocks*. London: Chapman & Hall. 217 p.

Taylor G. J., Keil K. and McCoy T. 1993. Asteroid differentiation: Pyroclastic volcanism to magma oceans. *Meteoritics* 28:34-52.

Terho M., Pesonen L. J. and Kukkonen I. T. 1993. The petrophysical classification of meteorites. *Studia Geophysica et Geodaetica* 37:65-82.

de Wall, H. 2000. The field-dependence of AC susceptibility in titanomagnetites: Implications for the anisotropy of magnetic susceptibility. *Geophysical Research Letters* 27(16):2409-2411.

Wilkison S. L, McCoy T. J., McCamant J. E., Robinson M. S. and Britt D. T. 2003. Porosity and density of ordinary chondrites: Clues to the formation of friable and porous ordinary chondrites. *Meteoritics and Planetary Science 38*(10):1533-1546.

Wilkison S. L. and Robinson M. S. 2000. Some bulk density measurements of ordinary chondrites. 31st *Lunar and Planetary Science Conference* (Abstract #1939). Houston, USA.

Worm, H-Ulrich. 1991. Multidomain susceptibility and anomalously strong low field dependence of induced magnetization in pyrrhotite. *Physics of the Earth and Planetary Interiors* 69:112-118.

Worm, H-Ulrich 1998. On the superparamagnetic – stable single domain transition for magnetite, and frequency dependence of susceptibility. *Geophysical Journal International* 133:201-206.

Worm, H-Ulrich, Clark D. and Dekkers M. J. 1993. Magnetic susceptibility of pyrrhotite: Grain size, field and frequency dependence. *Geophysical Journal International* 114:127-137.

Appendix I. Magnetic susceptibility values (Logχ in $10^{-8}m^3/kg$) of chondrites.

Meteorite	Comments	Mass (g)	Class	Logχ 19000 Hz	A%	B%	χ_{FD}%
Carbonaceous Chondrite							
Banten	c, Fall	3.81	CM2	4.10	5.0	-7.0	6.9
Cold Bokkeveld	c, Fall	2.95	CM2	3.34	-	-	9.2
Cold Bokkeveld	c, Fall	0.42	CM2	3.60	8.7	-8.6	15.5
Cold Bokkeveld	c, Fall	0.96	CM2	3.73	8.6	-5.8	8.6
Colony	c, Find	22.8	CO3	4.56	-	-	2.3
Coolidge	c, Find	1.59	C3.8-4	4.90	9.3	-3.5	3.8
Coolidge	c, Find	1.8	C3.8-4	4.90	9.8	-7.0	6.2
Isna	c, Find	4.22	CO3.8	4.39	8.6	-8.8	5.3
Karoonda	-, Fall	3.92	CK4	4.75	2.6	-0.6	2.6
Leoville	c, Find, R, long (6.8 cm)	25.1	CV3	4.43	-	-	0.6
Leoville	c, Find, R	4.05	CV3	4.60	9.7	-7.7	3.3
Loongana 001	c, Find	1.45	C3.8-4	4.92	8.2	1.2	7.8
Maralinga	c, Find, ANOM	1.08	CK4	4.64	3.3	-2.0	0.5
Mighei	c, Fall	6.92	CM2	3.51	4.0	-3.3	6.8
Murchison	c, Fall	11.18	CM2	3.46	5.1	-0.7	8.3
Murchison	C, Fall	3.26	CM2	3.92	4.8	-3.9	5.0
Murray	-, Fall	1.82	CM2	3.83	2.8	-3.4	8.8
Nogoya	C, Fall	1.72	CM2	3.56	1.8	-3.0	4.3
NWA 801'	*-, Find*	2.7	*CR2*	*5.16*	*26.5*	*20.4*	2.9
NWA 801	c, Find	8.6	CR2	4.91	7.9	-2.1	5.3
NWA 2086	-, Find	6.3	CV3	3.21	2.5	-2.2	6.0
NWA 1112	c, Find	0.6	CK5	4.74	6.6	-5.0	2.1
Ornans	-, Fall	3.82	CO3.4	4.22	2.3	-1.7	4.2
Warrenton	-, Fall	4.48	CO3.7	4.37	4.6	-6.7	2.5
Warrenton	c, Fall	16.42	CO3.7	4.45	-	-	-1.0
Enstatite Chondrite							
ABEE	c,Fall, imb.	13.66	EH4	5.51	28.4	19.7	4.8
ABEE	-,Fall, imb.	42.54	EH4	5.43	-	-	1.6
ABEE (matrix)	-,Fall, imb.	14.58	EH4	5.44	21.6	-3.6	6.4
Atlanta	C, Find	7.6	EL6	5.33	17.2	5.1	3.9
Blithfield	C, Find, saturation at 19000Hz	50.9	EL6	5.52*	-	-	-
Daniel's Kuil	c, Fall	1.02	EL6	5.70	33.8	12.5	12.6
Daniel's Kuil	c, Fall	0.38	EL6	5.59	30.5	22.5	10.8
Daniel's Kuil	-, Fall	0.2	EL6	4.55	-	-	14.2
Eagle	c, Find	30.22	EL6	5.51	-	-	7.9

Happy Canyon	c, Find, imb.	74.6	EL	4.38	-	-	6.4
Happy Canyon'	*c, Find, imb.*	*6.62*	*EL*	*3.62*	*5.6*	*1.5*	6.6
Indarch	c, Fall	2.17	EH4	5.45	32.3	-15.0	4.5
Indarch	c, Fall	1.7	EH4	5.45	30.3	-7.0	3.5
Indarch	-, Fall	0.36	EH4	5.35	28.2	14.0	13.5
Indarch	-, Fall	0.12	EH4	5.31	19.3	-3.7	9.4
Indarch	c, Fall	30.92	EH4	5.39	-	-	4.9
Khairpur	c, Fall	70.5	EL6	5.45	-	-	17.9
Pillisfter	c, Fall	27.55	EL6	5.70*	-	-	-
Yilmia	C, Find	11.37	EL6	4.83	7.2	-3.4	3.4

H Chondrite

Acfer 002	C, Find	20.74	H5	5.02	-	-	9.2
Acfer 005	c, Find	7.7	H3.9	5.09	18.8	-4.5	-2.8
Acfer 008	C, Find	12.17	H5	5.13	14.9	-14.1	8.4
Acfer 012	c, Find	13.15	H6	5.21	-	-	6.2
Allegan	-, Fall	10.32	H5	5.34	-	-	10.8
Aurora	c, Find	5.84	H4	5.10	23.3	-7.3	3.3
Bath	c, Fall, br, long (6.6 cm)	62	H4	5.31*	-	-	-
Beardsley	C, Fall	13.62	H5	5.20	20.8	-27.7	4.5
Beaver Creek	c, Fall	17.07	H4	5.28	-	-	5.3
Bur-Gheluai	c, Fall, xen	8.14	H5	5.30	-	-	-0.5
Burnabbie	C, Find	4.27	H5	4.70	-	-	9.9
Chamberlin	c, Find	5.78	H5	4.67	15.1	1.0	3.3
Chiang Khan	c, Fall	6.92	H6	5.33	21.7	-8.6	5.0
Correo	C, Find	45.26	H4	5.20	-	-	7.5
Dhofar 276	c, Find	7.57	H5	4.61	-	-	4.5
Djati-Pengilon	C, Fall	6.36	H6	4.96	-	-	12.0
Elsinora	c, Find, vnd	5.16	H5	5.14	18.4	-8.5	11.7
Ferguson Switch	c, Find	8.36	H5	5.14	22.9	1.2	10.2
Forest City	C, Fall, br	2.04	H5	5.29	7.9	-1.1	11.1
Forest City	C, Fall, br	1.84	H5	5.26	27.4	-9.9	11.0
Foster	c, Find	12.16	H4	4.81	5.8	4.4	3.1
Glanggang	c, Fall	15.14	H5/6	5.41	-	-	11.7
Grayton	c, Find	27.36	H5	4.85	-	-	4.3
Heredia	c, Fall, br, saturation at 19000 Hz	5.52	H5	5.50*	-	-	-
Hessle	C, Fall	2.24	H5	5.15	16.1	-11.9	6.6
Hessle	C, Fall	4.28	H5	5.24	17.9	-26.3	6.9
Hugo (stone)	c, Find	2.18	H5	5.08	19.0	-0.2	10.7
Ingella Station	*C, Find*	*34.52*	*H5*	*4.39*	-	-	*2.7*
Jilin	-, Fall	5.68	H5	5.43	-	-	12.7

Kesen	-, Fall	13.98	H4	5.36	-	-	6.3
Laundry East	*C, Find*	*4.3*	*H3.7*	*4.04*	-	-	*2.6*
Lewiston	c, Find, long (6.2 cm)	18.56	H4	4.61	-	-	0.7
Limerick	-, Fall, vnd, saturation at 19000 Hz	9.94	H5	5.47*	-	-	-
Meester-Cornelis	c, Fall, friable	18.18	H5	5.16	-	-	1.3
Miami	c, Find	11.1	H5	4.75	4.5	2.6	2.5
Mooresfort	c, Fall, xen	12.58	H5	5.32	-	-	2.5
Mulga (north)	C, Find	3.52	H6	4.93	-	-	8.2
Mulga (north)	C, Find	6.36	H6	5.09	-	-	6.1
Mulga (north)	C, Find	1.94	H6	5.13	-	-	7.5
Mulga (north)	c, Find	2.49	H6	5.13	-	-	10.0
Nardoo (no.1)	c, Find	31.1	H5	5.24	-	-	9.7
Nuevo Mercurio	C, Fall	0.5	H5	5.42	-	-	15.1
Nuevo Mercurio	C, Fall	0.62	H5	5.41	-	-	12.6
Nuevo Mercurio	C, Fall	0.35	H5	5.42	-	-	22.6
Nuevo Mercurio	C, Fall	0.44	H5	5.37	-	-	15.2
Nuevo Mercurio	C, Fall	1.88	H5	5.36	-	-	14.4
Nuevo Mercurio	C, Fall	1	H5	4.79	-	-	4.1
Nuevo Mercurio	C, Fall	1.2	H5	5.51	-	-	18.7
Nuevo Mercurio	C, Fall	1.46	H5	5.38	-	-	7.3
Nuevo Mercurio	C, Fall	0.7	H5	5.42	-	-	17.2
Nuevo Mercurio	C, Fall	0.58	H5	5.41	-	-	18.7
Nuevo Mercurio	C, Fall	0.98	H5	5.36	-	-	16.1
Nuevo Mercurio	C, Fall	1.62	H5	5.34	-	-	12.3
Nuevo Mercurio	C, Fall	2.38	H5	5.41	-	-	13.8
Nuevo Mercurio	C, Fall	4.7	H5	5.37	14.0	-4.4	10.2
Nuevo Mercurio	C, Fall	4.44	H5	5.23	26.2	16.1	17.2
Ochansk	-, Fall, br	1.22	H4	5.24	23.7	-8.9	18.6
Phum Sambo	c, Fall	3.12	H4	5.40	20.6	-13.2	14.2
Phum Sambo	c, Fall	2.36	H4	5.34	17.4	-19.1	17.0
Pultusk	C, Fall, vnd, br	9.84	H5	5.27	14.2	-22.5	5.5
Reggane 003	Find, too large for 19000 Hz	26.03	H4	5.11*	-	-	-
Republican River	c, Find	5.5	H4	4.48	8.6	-0.5	5.7
Richardton	C, Fall, vnd	12.22	H5	5.45*	20.3	-1.7	-
Roosevelt County 001	C, Find	5.67	H3.8	4.75	21.0	0.1	7.7
Roosevelt County 003	C, Find	5.04	H5	4.70	2.9	-0.4	3.9
Roosevelt County 007	C, Find	3.32	H5	4.53	3.5	-0.5	4.5
Roosevelt County 009	C, Find	0.16	H5	4.79	21.9	-33.9	11.5
Roosevelt County 012	c, Find	2.68	H5	4.37	8.9	2.0	1.9
Roosevelt County 018	c, Find	1.2	H5	4.77	9.0	-4.2	7.2
Roosevelt County 023	C, Find	10.32	H5	4.79	-	-	7.7

Roosevelt County 024	*c, Find*	*0.72*	*H5*	*4.44*	*15.6*	*0.8*	*12.2*
Roosevelt County 073	C, Find	6.88	H5	4.78	14.0	-19.9	3.4
Sand Draw	c, Find	7.44	H5	5.21	23.9	14.3	17.0
Sindhri	-, Fall	1.11	H5	5.24	-	-	8.0
Texline	c, Find	12.26	H5	5.31	-	-	-0.5
Torrington	c, Fall	8.64	H6	5.45	-	-	19.5
Tromoy	c, Fall	6.3	H	5.38	11.0	-12.5	9.9
Ute Creek	C, Find	18.86	H4	5.19	-	-	2.2
Warden	c, Find	10.7	H5	5.29	-	-	12.3
West Forrest	C, Find	6.86	H5	4.82	-	-	3.1
Wiluna	C, Fall	5.23	H5	5.37	21.1	9.1	16.0
Wiluna	C, Fall	5.46	H5	5.22	11.8	-10.0	5.9
Wiluna	C, Fall	7.58	H5	5.30	9.1	-1.7	12.4
Wiluna	C, Fall	3.4	H5	5.21	14.4	-14.9	10.5
Zhovtnevyi	c, Fall	12.8	H5	5.30	18.7	-2.0	25.2

L Chondrite

Acfer 001	c, Find	16.44	L6	5.00	18.3	-11.4	2.5
Aleppo	c, Fall, br	2.4	L6	4.69	-	-	5.5
Alfianello	c, Fall	33.28	L6	4.91	-	-	2.5
Atemajac	c, Fall	4.06	L6	4.88	-	-	3.0
Barwell	c, Fall	3.52	L6	4.89	12.0	-0.7	14.6
Bath Furnace	c, Fall	17.29	L6	4.89	-	-	4.8
Billygoat Donga	c, Find	3.76	L6	4.98	-	-	3.1
Bruderheim	c, Fall	122.8	L6	4.94*	-	-	-
Bruderheim	c, Fall	88.2	L6	4.98*	-	-	-
Bruderheim	c, Fall	39.74	L6	5.14*	-	-	-
Bruderheim	c, Fall	26	L6	4.88	-	-	-
Bruderheim	c, Fall	2.7	L6	4.96	27.5	-11.2	-
Bruderheim	c, Fall	18.4	L6	4.94	-	-	-
Bruderheim	c, Fall	7	L6	4.77	14.2	-17.6	-
Bruderheim	c, Fall	10.6	L6	4.99	15.5	-24.7	-
Bruderheim	c, Fall	9.2	L6	4.96	15.7	-22.7	-
Bruderheim	c, Fall	17.1	L6	4.88	-	-	-
Cilimus	C, Fall	17.56	L5	4.94	-	-	7.9
Coorara	c, Find	3.36	L6	4.26	-	-	4.6
Denver	C, Fall	15.08	L6	4.80	-	-	4.2
Elenovka	-, Fall	11.18	L5	4.84	5.2	-0.4	13.0

Erie	c, Find, too large for 19000 Hz	39.94	L6	4.65*	-	-	-
Farmington	c, Fall, br, blk, long (7.3cm)	31.24	L5	4.92	-	-	-0.1
Floyd	c, Find	8.92	L4	4.85	23.3	-16.3	-1.0
Homestead	c, Fall, br.	13.5	L5	4.90	-	-	4.2
Honolulu	c, Fall, vnd	4.66	L5	4.78	12.4	-8.3	13.7
Isoulane-n-Amahar	c, Find, vnd., long (7.0cm)	55.42	L6	4.76	-	-	1.5
Johnson City	c, Find	8.11	L6	4.59	-	-	-0.9
Jumapalo	c, Fall	5.94	L6	4.73	27.0	-3.3	20.2
Kendleton	C, Fall, br	14.14	L4	4.83	-	-	10.7
Kyushu	C, Fall, vnd	21.4	L6	4.95	-	-	3.3
La Criolla	C, Fall	68	L6	4.73	-	-	14.6
La Criolla	C, Fall	9.46	L6	4.76	-	-	1.3
La Criolla	C, Fall	3.08	L6	4.85	-	-	11.4
Leedey	c, Fall	14.26	L6	4.93	17.8	5.5	7.1
Lubbock	c, Find	6	L5	4.85	8.8	-5.2	5.3
Lushton	*c, Find*	*27.1*	*L6*	*3.76*	-	-	*-1.1*
Mauerkirchen	c, Fall	5.96	L6	4.82	13.3	-15.2	6.1
Mocs	C, Fall, vnd	4.03	L6	4.82	5.6	1.1	10.3
Moorabie	*c, Find*	*6.9*	*L3.8*	*5.35*	-	-	*3.2*
Mossgiel	C, Find	13.12	L4	3.88	-	-	-1.1
Nerft	c, Fall, vnd	23.54	L6	5.01	-	-	1.1
New Concord	c, Fall, vnd	26.76	L6	4.92	-	-	-1.6
Peace River	-, Fall	11.62	L6	4.95	-	-	3.0
Peace River	-, Fall	0.32	L6	4.90	18.7	-20.4	-3.8
Roosevelt County 002	C, Find	2.94	L6	4.46	17.4	-4.3	11.9
Roosevelt County 004	*C, Find*	*2.76*	*L6*	*3.49*	*9.5*	*-0.9*	*6.3*
Roosevelt County 017	*C, Find*	*10.96*	*L6*	*3.48*	-	-	4.7
Roosevelt County 019	c, Find	13.56	L5	4.29	-	-	2.4
Roosevelt County 020	C, Find	2.01	L5	4.40	2.9	-2.9	5.9
Roosevelt County 025	c, Find	0.46	L5	4.35	18.3	-21.2	7.2
Roosevelt County 066	C, Find	0.2	L5	3.94	8.0	0.1	11.1
Roosevelt County 067	C, Find	0.18	L5	3.92	13.3	0.9	11.7
Roosevelt County 069	C, Find	4.19	L5	4.30	12.6	-23.7	5.6
Roosevelt County 070	C, Find	0.66	L5	4.13	18.3	6.1	2.2
SaU 001	c, Find	19.5	L4/5	4.65	-	-	2.3
Shelburne	c, Fall, vnd, br	16.3	L5	5.02	-	-	6.2
Smith Center	c, Find	3.24	L6	4.38	12.4	-16.1	3.1
Summerfield	-, Find	36.34	L5	3.87	-	-	3.9
Tadjera	-, Fall, blk	9.76	L5	4.95	21.8	-14.0	8.3
Tarbagatai	C, Find	9.88	L5	4.69	19.8	-33.3	0.9
Tenham	C, Fall, vnd, large	113	L6	4.73*	-	-	-

Tenham	C, Fall, vnd	14.26	L6	4.83	-	-	3.4
Tjerebon	c, Fall	8.5	L5	4.85	-	-	9.5
Umbarger	c, Find	20.78	L3/6	4.30	4.4	0.2	2.4
Wah Wah Valley	C, Find	2.2	L6	4.44	6.4	-5.8	5.2
Waldo	c, Find	3.92	L6	4.36	6.8	-2.9	4.3
Woolgorong	c, Fall	9.62	L6	4.75	-	-	8.8
Wooramel	c, Find	7.16	L5	4.67	-	-	3.5

LL Chondrite

Bandong	c, Fall	4.56	LL6	3.73	9.1	-11.9	0.9
Benton	c, Fall	2.02	LL6	3.58	6.5	-10.3	8.6
Greenwell Springs	c, Find	3.5	LL4	4.29	5.4	0.6	5.5
NWA 872	c, Find	8.6	LL3	4.08	-	-	1.6
NWA 1279	-, Find	3.3	LL3.7	3.68	10.3	-16.9	2.2
NWA 1930	-, Find	5.5	LL3	4.62	16.0	1.6	2.5
NWA 1945	c, Find	3.5	LL3	4.22	10.1	-10.3	4.2
Tuxtuac	-, Fall	2.68	LL5	4.14	4.9	-0.8	3.9

Intermediate Ordinary Chondrite

Bremervorde	c, Fall, br	7.7	H/L3.9	5.07	15.8	-6.9	-4.6
Cynthiana	c, Fall, set in epoxy	~2	L/LL4	3.85	3.8	-3.6	3.5
Cynthiana	c, Fall	14.2	L/LL4	4.58	-	-	5.2
Knyahinya	C, Fall, br., too large for 19000 Hz	143	L/LL5	5.37*	-	-	-
Knyahinya	C, Fall, br.	18.44	L/LL5	4.68	19.8	-38.3	0.6
Knyahinya	C, Fall, br	2.78	L/LL5	4.66	29.7	-22.8	1.2

Rumurutiite

NWA 753	c, Find, long (7.0 cm)	19.5	R3.9	2.86	-	-	5.9
NWA 1668	c, Find	3.4	R5	2.97	3.5	-3.5	5.9

Unclassified Meteorites

Acfer 057	C, Find, long (6.0 cm)	120.7	L?	3.78*	-	-	-
Red Lake	C, Find	1.58	?	4.62	11.1	-4.1	3.9

C: >50% fusion crust, c: <50% fusion crust, - : no crust present
Class abbreviations and following comments from Jensen et al. (2004).
br: brecciated, imb: impact melt breccia, vnd: veined, xen: xenolithic, blk: black, R: reduced.
* 825 Hz measurement taken.
Outlier specimens are in italics.

Appendix II. Magnetic susceptibility values (Logχ in $10^{-9} m^3/kg$) of achondrites.

Meteorite	Comments	Mass (g)	Class	Logχ 19000 Hz	A%	B%	χ_{FD}%
Primitive Achondrite							
NWA 725	c, Find	2.7	ACA	5.70	33.7	-31.5	25.6
Haverö	-, Fall	1.87	URE	5.10	13.2	9.4	4.3
Hughes 007	-, Find	0.34	URE	4.31	2.6	-1.0	3.9
Hughes 009	C, Find	1.6	URE	4.17	6.9	3.0	5.4
Kenna	c, Find	22.4	URE	4.57	-	-	-0.9
Kenna	c, Find	6.78	URE	4.53	-	-	2.6
Nova 001	C, Find	18.22	URE	4.83	17.5	14.0	6.5
Tierra Blanca	C, Find	15.72	WIN	4.41	-	-	2.6
Aubrite							
Bishopville	c, Fall	0.6	AUB	3.09	50.1	-5.3	-
Bishopville	-, Fall	0.26	AUB	3.01	34.2	20.8	11.5
Cumberland Falls	c, Fall	7.2	AUB	4.60	-	-	8.9
Khor Temiki	-, Fall	1.2	AUB	3.21	53.3	36.1	17.1
Mayo Belwa	c, Fall	0.94	AUB	3.70	32.5	19.6	2.4
Norton County	c, Fall	32.28	AUB	3.28	-	-	13.5
Norton County	C, Fall	3.1	AUB	3.77	-	-	4.2
Norton County	-, Fall	10.86	AUB	3.05	29.0	12.9	8.0
Peña Blanca Spring	c, Fall	14.66	AUB	2.86	-	-	1.0
Pesyanoe	c, Fall	2.86	AUB	3.57	15.2	0.6	5.6
Brachinite							
Eagles Nest	c, Find	1.2	BRA	3.33	10.7	-14.7	9.4
Howardite							
Kapoeta	-, Fall, friable	1.1	HOW	3.04	2.8	-1.9	1.0
Luotolax	-, Fall, friable	2.86	HOW	3.19	8.5	1.7	1.8
Eucrite							
Camel Donga	c, Find, br	6.54	EUC	4.66	-	-	6.5
Camel Donga	C, Find, br	3.97	EUC	4.33	-	-	4.0
Camel Donga	C, Find, br	1.5	EUC	4.01	-	-	8.7
Camel Donga	C, Find, br	1.7	EUC	4.06	-	-	1.8
Camel Donga	C, Find, br	9.67	EUC	3.98	-	-	1.1
Camel Donga	C, Find, br	11.74	EUC	4.34	15.8	-23.0	4.9

Camel Donga	C, Find, br	10.5	EUC	4.29	15.5	-17.5	6.0
Camel Donga	C, Find, br	7.34	EUC	4.34	12.8	-16.0	5.4
Camel Donga	C, Find, br	5.84	EUC	4.08	13.9	-16.9	9.5
Camel Donga	C, Find, br	3.66	EUC	4.39	-	-	-0.7
Camel Donga	C, Find, br	6.06	EUC	4.33	-	-	5.5
Camel Donga	C, Find, br	13.42	EUC	4.32	-	-	3.1
Juvinas	c, Fall, mbr.	4.46	EUC	3.11	8.4	-8.8	2.8
Millbillillie	C, Fall	3.54	EUC	2.67	-	-	-
Millbillillie	C, Fall	5.76	EUC	2.70	-	-	-
Millbillillie	C, Fall	5.48	EUC	2.63	-	-	-
Millbillillie	C, Fall	8.6	EUC	2.71	0.5	0.3	-
Millbillillie	C, Fall	5.94	EUC	2.74	-	-	-
Millbillillie	C, Fall	6.57	EUC	2.61	-	-	-
Millbillillie	C, Fall	7.58	EUC	2.73	-	-	-
Millbillillie	C, Fall	9.8	EUC	2.80	-	-	-
Millbillillie	C, Fall	9.66	EUC	2.64	-	-	-
Millbillillie	C, Fall	11	EUC	2.68	-	-	-
Millbillillie	C, Fall	4.86	EUC	2.65	-	-	-
Millbillillie	C, Fall	6.46	EUC	2.65	-	-	-
Millbillillie	C, Fall	7.18	EUC	2.69	-	-	-
Millbillillie	C, Fall	6.28	EUC	2.76	-	-	-
Millbillillie	C, Fall	8.8	EUC	2.62	-	-	-
Millbillillie	C, Fall	13.34	EUC	2.73	-	-	3.1
Millbillillie	C, Fall	15.92	EUC	2.64	-	-	2.7
Millbillillie	C, Fall	13.75	EUC	2.64	1.2	0.2	2.4
Millbillillie	C, Fall	11.15	EUC	2.73	-	-	3.0
Millbillillie	C, Fall	19.4	EUC	2.64	-	-	3.0
Millbillillie	C, Fall	3.53	EUC	2.66	-	-	4.8
Millbillillie	C, Fall	5.94	EUC	2.72	-	-	3.3
Millbillillie	C, Fall	19.14	EUC	2.65	-	-	2.7
Millbillillie	C, Fall	4.3	EUC	2.78	-	-	3.2
Millbillillie	C, Fall	8.22	EUC	2.62	-	-	3.2
Millbillillie	C, Fall	5	EUC	2.61	-	-	1.0
Millbillillie	C, Fall	7.1	EUC	2.66	-	-	4.4
Millbillillie	C, Fall	6.42	EUC	2.61	-	-	4.5
Millbillillie	C, Fall	10.11	EUC	2.60	-	-	3.7
Millbillillie	C, Fall	5.04	EUC	2.70	-	-	4.5
Millbillillie	C, Fall	4.94	EUC	2.88	-	-	5.5
Millbillillie	C, Fall	9.08	EUC	2.68	-	-	4.5
Millbillillie	C, Fall	7.22	EUC	2.68	-	-	5.7
Millbillillie	C, Fall	12.7	EUC	2.62	-	-	3.5

Millbillillie	C, Fall	22.98	EUC	2.68	-	-	1.0
Millbillillie	C, Fall	17.72	EUC	2.64	-	-	2.3
Millbillillie	C, Fall	15.54	EUC	2.61	-	-	2.2
Millbillillie	C, Fall	19.16	EUC	2.63	-	-	2.2
Millbillillie	C, Fall	22.92	EUC	2.63	-	-	0.5
Millbillillie	C, Fall	33.2	EUC	2.63	-	-	6.2
Millbillillie	C, Fall	3.7	EUC	2.63	-	-	2.7
Millbillillie	C, Fall	3.9	EUC	2.75	-	-	3.2
Millbillillie	C, Fall	36.88	EUC	2.62	-	-	-1.6
Millbillillie	C, Fall	50.04	EUC	2.62	-	-	3.6
Millbillillie	C, Fall	20.5	EUC	2.68	-	-	-0.4
Millbillillie	C, Fall	25.08	EUC	2.66	-	-	0.0
Millbillillie	C, Fall	15.22	EUC	2.67	-	-	2.4
Millbillillie	C, Fall	4.28	EUC	2.65	3.6	0.5	6.3
Padvarninkai	C, Fall, mbr.	9.72	EUC	2.84	5.2	-6.4	0.5
Palo Blanco Creek	c, Find	8.09	EUC	2.87	10.7	-8.1	4.3
Pasamonte	c, Fall, pmb.	7.7	EUC	2.96	-	-	5.5
Stannern	c, Fall, mbr, friable	5.62	EUC	2.71	2.6	-0.6	3.9
Stannern	c, Fall, mbr, friable	4.2	EUC	2.67	-	-	5.1
Stannern	c, Fall, mbr, friable	1.38	EUC	2.66	3.0	-1.5	-
Stannern	c, Fall, mbr, friable	2.82	EUC	2.67	3.3	-3.0	-

Diogenite

Johnstown	c, Fall	48.74	DIO	3.30	-	-	9.1
Johnstown	C, Fall	13.84	DIO	3.71	19.9	8.0	10.5

SNC meteorite

Chassigny	c, Fall	2.58	CHA	3.06	8.2	-10.8	2.1
DaG 489	-, Find	0.33	SHE	2.90	10.8	6.4	-
Dhofar 019	c, Find	0.156	SHE	2.68	-	-	-
Nakhla	c, Fall	25.3	NAK	3.23	-	-	0.7
Nakhla	c, Fall	0.62	NAK	3.28	2.9	2.5	-0.2
NWA 1068	-, Find	0.3	SHE	3.23	3.5	0.0	9.3
NWA 1195	c, Find	0.212	SHE	3.01	-	-	-
Shergotty	c, Fall	0.82	SHE	3.21	3.6	-0.3	9.6
Zagami	Fall	10.8	SHE	2.68	-	-	3.2
*Zagami	-, Fall	0.22	SHE	2.83	-	-	-
*Zagami	c, Fall	0.098	SHE	2.81	-	-	-

Lunaites							
*Dhofar 461	-, Find	0.123	LUN	2.37	-	-	-
*Lunar Soil	grains in capsule from Apollo 11	0.01	LUN	3.65	-	-	-

C: >50% fusion crust, c: <50% fusion crust, - : no crust present.
Class abbreviations and following comments from Jensen et al. (2004).
br: brecciated, mbr: monomict breccia, pmb: polymict breccia, vnd: veined, xen: xenolithic, blk: black.
* see section 2.1 in text.

Appendix III. Magnetic susceptibility values (Logχ in $10^{-9}m^3/kg$) of stony irons

Meteorite	Comments	Mass (g)	Class	Logχ 825 Hz	A%	B%	χ_{FD}%
Mesosiderite							
Mincy	c, Find, long (6.0 cm)	56.63	MES	6.13	-	-	-

C: >50% fusion crust, c: <50% fusion crust, - : no crust present.
Class abbreviations from Jensen et al. (2004).